CONSOLIDATION OF AEROSPACE GRADE ALUMINUM 7055 POWDER VIA PM TECHNOLOGIES

by

Neal P. Kraus

Submitted in partial fulfilment of the requirements
for the degree of Master of Applied Science

at

Dalhousie University
Halifax, Nova Scotia
August 2016

TABLE OF CONTENTS

LIST OF TABLES

LIST OF FIGURES

ABSTRACT

The objective of this research was to assess the response of aerospace grade gas atomized aluminum 7055 (Al-8Zn-2.1Mg-2.3Cu-0.2Zr) powder to sinter-forge and SPS-forge styles of powder metallurgy processing. In meeting this objective the powder was processed through a three-stage sequence of cold isostatic pressing, liquid phase sintering, and rotary forging or through a two stage sequence of spark plasma sintering and rotary forging. In the prior, core variables included sintering temperature, particle size, the effects of admixed sintering activators (Mg, Sn), and forging temperature. Here it was found that the removal of fines (x<45μm) was required to ensure a crack free product while forging. It was also observed that while tin helped to produce a sintered product with higher density, the addition was detrimental to the post-forged mechanical properties. Overall it was found that a sintering temperature of 580°C and a forging temperature of 470°C, produced a fully dense product with wrought like tensile properties and hardness. In SPS-based research, core variables included sintering temperature, sintering time, and the timing of the application of pressure. Here it was found that the bend properties of sintered products were substantially higher when pressure was applied in a Type II mode of pressure application (pressure applied once the compact was at full temperature). Overall a sintering temperature of 500°C was found to produce products with the highest strength along with a sintering time of 2400 seconds. Once the sintered billets were forged and heat treated, products were found to be fully dense and have wrought like tensile properties and hardness. In both cases forging of the CIP-Sinter and SPS'ed products greatly increased the tensile properties of the product and was believed to help break up and refine the oxide shell present on the aluminum particles to a point where this constituent was dispersed within the material and thereby acted as a strengthening agent within the product.

LIST OF ABBREVIATIONS USED

ASTM	American Society for Testing and Materials
CAPAD	Current Activated, Pressure-Assisted Densification
CIP	Cold Isostatic Pressing
DC	Direct Current
DSC	Differential Scanning Calorimetry
EBSD	Electron Back Scatter Diffraction
ECAS	Electric Current Activated Sintering
EDS	Energy-Dispersive X-Ray Spectroscopy
EPAC	Electric Pulse Assisted Consolidation
GP Zones	Guinier-Preston Zones
GC-MS	Gas Chromatography-Mass Spectrometry
HAGB	High Angle Grain Boundary
HRB	Rockwell Hardness: Scale B
ICP-OES	Inductively Coupled Plasma – Optical Emission Spectroscopy
LAGB	Low Angle Grain Boundary
LPS	Liquid Phase Sintering
MMC	Metal Matrix Composite
MPa	MegaPascal
MPIF	Metal Powder Industries Federation
PECS	Pulsed Electric Current Sintering
PM	Powder Metallurgy
ppm	Parts per million
SEM	Scanning Electron Microscope
SPS	Spark Plasma Sintering
SSLPS	Super Solidus Liquid Phase Sintering
SSSS	Super Saturated Solid Solution
TGA	Thermogravimetric Analysis
T7	Temper Designation: Solution-treated and stabilized by overaging
UBS	Ultimate Bend Strength
UDC / UNI	Uniaxial Die Compaction
UTS	Ultimate Tensile Strength
VRC	Vacancy Rich Cluster

ACKNOLEDGMENTS

The authors would like to graciously acknowledge the financial support provided by Boeing Research and Technology (research contract 11-6392), the Natural Sciences and Engineering Research Council of Canada (NSERC) via collaborative research and development grant #451466 and GKN Sinter Metals. Technical guidance provided by researchers at Boeing (Drs. Steve Gaydos, Ryan Glamm, Marc Froning) is also gratefully acknowledged as is the laboratory assistance provided by colleagues at Dalhousie University (Randy Cooke, Mark Amegadzie, Dean Grijm) and the powder atomization completed by Dr. Bernd Mais (Ecka Granules).

CHAPTER 1. INTRODUCTION

1.1 7xxx Series Aluminum Alloys

Wrought aluminum alloys have been classified into eight different series based on principal alloying additions. Because of these classifications, alloys within each series although having different chemistries, can have similar properties. Each series has been sub-divided in accordance with the "International Alloy Designation System" and utilizes a four digit coding system. In each case the first numeric value in alloy code designates which of the eight series the alloy belongs to, and thus, what its major alloying addition is. A table of the eight different series and their principal alloying elements is presented in Table 1.

Of the eight different series, the 2xxx and 7xxx series are those most often encountered in aerospace applications due to their ability to be precipitation hardened to very high strengths. Currently the 7xxx series, which is the series used to designate zinc as the major alloying element, is the series that can be precipitation strengthened to some of the highest strengths of all aluminum alloys.

Table 1: Aluminum wrought alloy numbering system [1].

Principle Alloying Element(s)	Series	Notes
Aluminum (≥ 99.00)	1xxx	Non Heat Treatable
Copper	2xxx	Heat Treatable
Manganese	3xxx	Non Heat Treatable
Silicon	4xxx	Non Heat Treatable
Magnesium	5xxx	Non Heat Treatable
Magnesium and Silicon	6xxx	Heat Treatable
Zinc	7xxx	Heat Treatable
Other Elements	8xxx	

1.1.1 Chemistry and Strengthening Mechanisms

7xxx series aluminum alloys are those that contain zinc as the major alloying element. In most cases the amount of zinc is between four and eight percent by mass. Although zinc is the main alloying constituent, it is rarely added as the sole addition. Other common alloying

elements used in the 7xxx series alloys are copper, magnesium, and zirconium, while some other members of this series also employ manganese and chromium [2].

All members of the 7xxx are strengthened through heat treatment denoted as age hardening or more commonly, precipitation hardening. For this to occur, specific conditions must be met. First of all, one or more of the principal alloying additions must exhibit a high solid solubility in aluminum at an elevated temperature. This must then decreases rapidly as the temperature is lowered so as to yield a super saturated solid solution (SSSS). The second requirement is that there must be an intermetallic phase present that can precipitated out of the SSSS. In most instances precipitation is executed in a single, isothermal step. However, in select alloys a multi-step process is employed to first nucleate and then grow the strengthening precipitates [3].

A schematic illustrating an exemplary heat treatment process as it pertains to the Al-Cu system is shown in Figure 1. Initially, the alloy is heated into a region above the solvus temperature (point (1)) where it is held for a prescribed period of time, typically on the order of 1-2 hours. At this stage alloying additions are diffused into the α-aluminum grains so as to produce a homogeneous solid solution state. The temperature is then dropped quickly though a quenching step yielding a non-equilibrium SSSS state at room temperature. Then through either natural (room temperature), or artificial (elevated temperature ~120 to 200°C) aging the alloy tries to reach an equilibrium state, thereby prompting the precipitation of secondary phase (intermetallic) that strengthens the alloy. Aging can be conducted under a number of temperatures/times with the most appropriate parameters varying with alloy chemistry. For example, curves that depict the corresponding transitions in tensile properties for a 7xxx series alloy are shown in Figure 2.

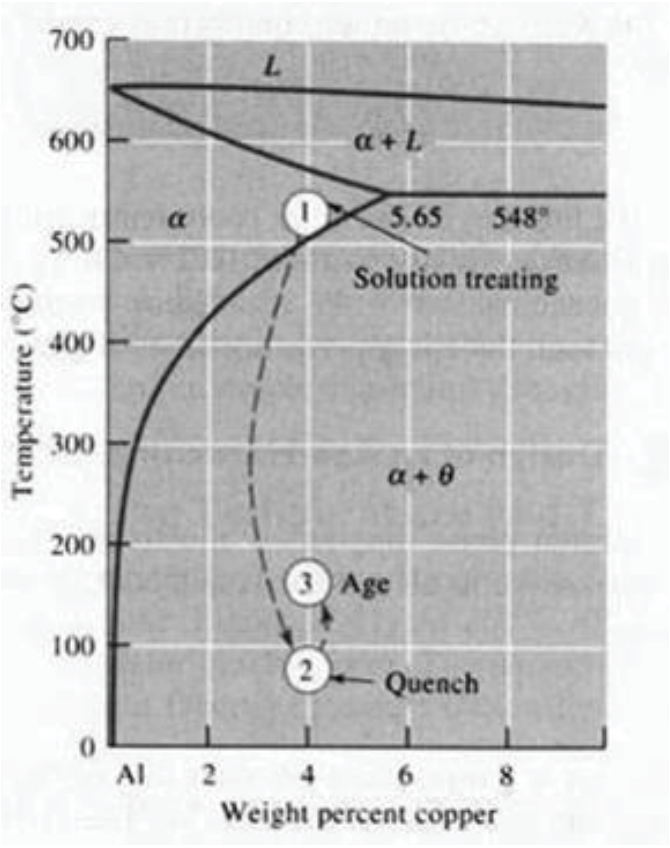

Figure 1: A typical sequence for precipitation hardening.

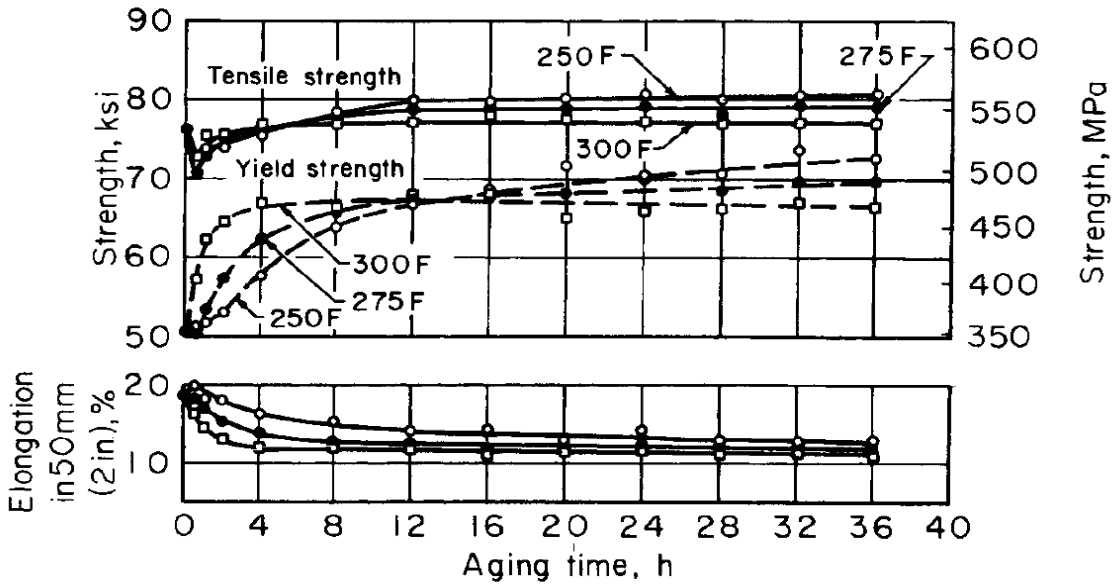

Figure 2: Aging curves devised for 7055 sheet when held at 120 to 150°C (250 to 300°F) [4].

When looking at the 7xxx series alloys and more specifically those within the Al-Zn-Cu-Mg category (i.e. 7055) a number of different precipitates can be formed during the ageing process. This includes η($MgZn_2$), T($Al_2Mg_3Zn_3$), S(Al_2CuMg) and θ(Al_2Cu) [5] and precursory meta-stable variants thereof. However, the most prevalent within 7xxx series alloys is the η phase. It has been frequently suggested that this particular phase is precipitated through a four stage sequence:

SSSS → GP zones → η' → η [6][7][8]

Although aspects of this process certainly remain in question [9], in this sequence Guinier-Preston (GP) zones are first formed in the SSSS lattice structure. GP zones, first recognised by Guinier [10] and Preston [11] in 1938, are finite areas which contain a high concentration of the solute atoms. GP zones are meta-stable, fully coherent with the parent lattice matrix, very small in size, and have a nominally spherical shape [12]. The η' phase is also metastable but is only semi-coherent. It has a definitive crystallographic structure (hexagonal unit cell with lattice values of a=0.496 and c=1.402 nm) and is regarded as the principal hardening phase in commercial Al-Zn-Mg alloys. With extended aging times, η' transforms into the η phase [13]. This phase is also hexagonal (a=0.5221 and c=0.8567 nm) but is completely incoherent [6].

Depending on how the alloy was quenched and the aging process applied, it has been noted that there are in fact two types of GP Zones with different structures; namely, GPI and GPII. GPI zones are fully coherent ordered zones containing Zn and Al or Mg on the $\{001\}_{Al}$ plane and can be produces over a wide range of temperatures, from room temperature up to 140 - 150 °C independently of quenching temperature [13]. GPII zones on the other hand are Zn-rich layers on the $\{111\}_{Al}$ plane that have been shown to be formed when quenching from temperatures above 450 °C and aged above 70 °C [13]. Hence, variations of the traditional sequence described above have been proposed. For instance, Ryum [14] has postulated that the core precipitation sequences include:

SSSS → GPI zones → η' → η

And

SSSS → VRC → η' → η

Vacancy-rich clusters or "VRC" are said to be formed during quenching and relate to the presence of a high concentration of quenched in vacancies within the microstructure. Building on this, Stiller et al. [15] [16] and Li et al. [17] have both proposed that the VRC clusters are precursors to GPII zones and that the nucleation sequence is actually:

SSSS → VRC → GPII → η' → η

While there are clearly differing opinions about GPI [18] and GPII [6] zones, both of these phases are presented to be precursors to the η' phase [17] and have been shown to have a marked effect on both the metastable and stable precipitates [19].

Copper also has been shown to play a role in the ultimate mechanical properties achieved. Within the 7xxx series aluminum alloys, the copper content is generally no higher than 2.3% [20]. Copper was originally added to the 7xxx series to help increase resistance to stress corrosion cracking (SCC)[21] [22]. However, it can also invoke precipitation of the θ phase and/or S phase so as to augment the strengthening achieved through η-based reactions. Copper can also impart solid solution strengthening [12] and can occupy Zn positions in the η' precipitates [23] so as to modify its properties and net strengthening capacity.

1.1.2 Characteristics of Wrought 7055 and Similar Alloys

The Al-Zn-Mg-(Cu) 7xxx series of aluminum alloys have been widely used in the aerospace industry thanks to their advantageous mechanical properties [24] [25]. Such alloys are employed in a wide variety of uses ranging from the skin of the plane and rivets, to structural parts. There are also many different alloys of the copper-rich (> 1% Cu) 7xxx series that are used in commercial aircraft including AA7050, AA7150, AA7X49 and AA7055 [26]. Such alloys are generally used for structural aerospace components because of their high strength, low weight and resistance to SCC.

An overview of the heat treatments that can be applied to aluminum alloys is shown in Table 2. While many options are clearly possible, 7xxx series alloys utilized in aerospace applications are frequently processed into a T7-type of temper because of their susceptibility to SCC. Within this temper there are many different heat treatment profiles that have been developed for different alloys. For instance the T73 temper was used to help improve the SCC resistance of 7075 plate in the short-transverse direction, while the T76 temper was applied to 7075 and 7178 to help improve the resistance to exfoliation corrosion. Since then, many other tempers in the T7x series have been developed and optimised for specific alloys and corrosion resistances [4]. The T76 temper series has expanded into other similar Cu-rich alloys such as 7050 and 7055; the chemical compositions of which are listed in Table 3.

Table 2: Overview of the heat treatment sequences commonly applied to aluminum alloys [12].

Temper	Process Description
T1	Cooled from the fabrication temperature and naturally aged
T2	Cooled from the fabrication temperature, cold worked, and naturally aged
T3	Solution-treated, cold-worked, and naturally aged
T4	Solution-treated and naturally aged
T5	Cooled from fabrication temperature and artificially aged
T6	Solution-treated and artificially aged
T7	Solution-treated and stabilized by overaging
T8	Solution-treated, cold-worked, and artificially aged
T9	Solution-treated, artificially aged, and cold-worked
T10	Cooled from the fabrication temperature, cold-worked and artificially aged

Table 3: Chemical composition limits for select 7xxx aluminum alloys [27].

Material Balance (wt. %)							
Alloy	Al	Zn	Mg	Cu	Zr	Fe	Cr
7050	Bal	5.7 – 6.7	1.9 – 2.6	2.0 – 2.6	0.08 – 0.12	0.15	0.04
7055	Bal	7.6 – 8.4	1.8 – 2.3	2.0 – 2.6	0.08 – 0.25	0.15	0.04
7075	Bal	5.1 – 6.1	2.1 – 2.9	1.2 – 2.0	---	0.50	0.18 – 0.28

Alloys 7050 and 7055 both use a similar heat treatment process under the T76x umbrella. In the case of 7050 the heat treatment applied is called T7651 and the newly developed heat treatment for 7055 is T76511. Both of these heat treatments are premised on the fact that selective corrosion at grain boundaries is reduced with increased overaging; in particular, their sensitivity to exfoliation corrosion [4]. Tensile properties for these select alloys are shown in Table 4.

Table 4: Tensile properties for select 7xxx aluminum alloys [2].

Alloy	E (GPa)	YS (MPa)	UTS (MPa)	Elongation (%)
7050 – T7651	72	490	550	11
7055 – T76511	71	575	616	10

1.2 Conventional Aluminum Powder Metallurgy Processing

Powder Metallurgy (PM) is a widely used manufacturing technology capable of fabricating parts with tight dimensional tolerances in high annual volumes. Because of these two facts most of the production of PM parts is centered around the automotive industry. However, PM is also applicable to the aerospace industry because of the capability to produce "impossible chemistries" which cannot be attained through normal production methods because of solubility constraints.

When considering the production of PM parts the underlying process involves three key stages as shown in Figure 3. Each of these stages are discussed in the following sections.

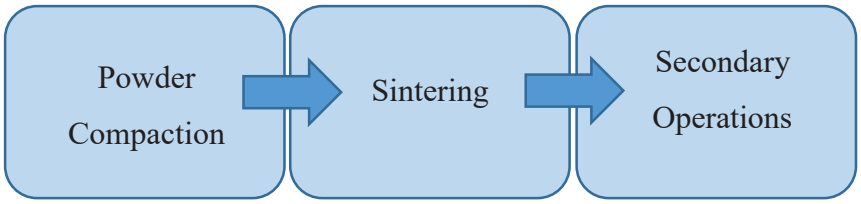

Figure 3: General flow diagram of the PM production process.

1.2.1 Powder Compaction

In conventional PM production a powder compaction step is initially applied to instill a prescribed part geometry with a particular density. When the part is first compacted it is only the mechanical bonds formed between the particles that are holding it together, at this stage it is said to be a green part. A green part has no usable mechanical properties and is just strong enough to be handled without fracture or chipping prior to sintering.

When looking at the production of green parts two main compaction techniques are utilized; namely, Uniaxial Die Compaction (UDC) and Cold Isostatic Pressing (CIP). In UDC pressure is typically applied to the powder along one axis only. It is the most common compaction technique and can be readily implemented as a fully automated process. In this approach a die is filled with powder to an initial set height and compacted along one axis

into a coherent green body. The part is then ejected and the process is repeated. A general schematic for UDC can be seen in Figure 4.

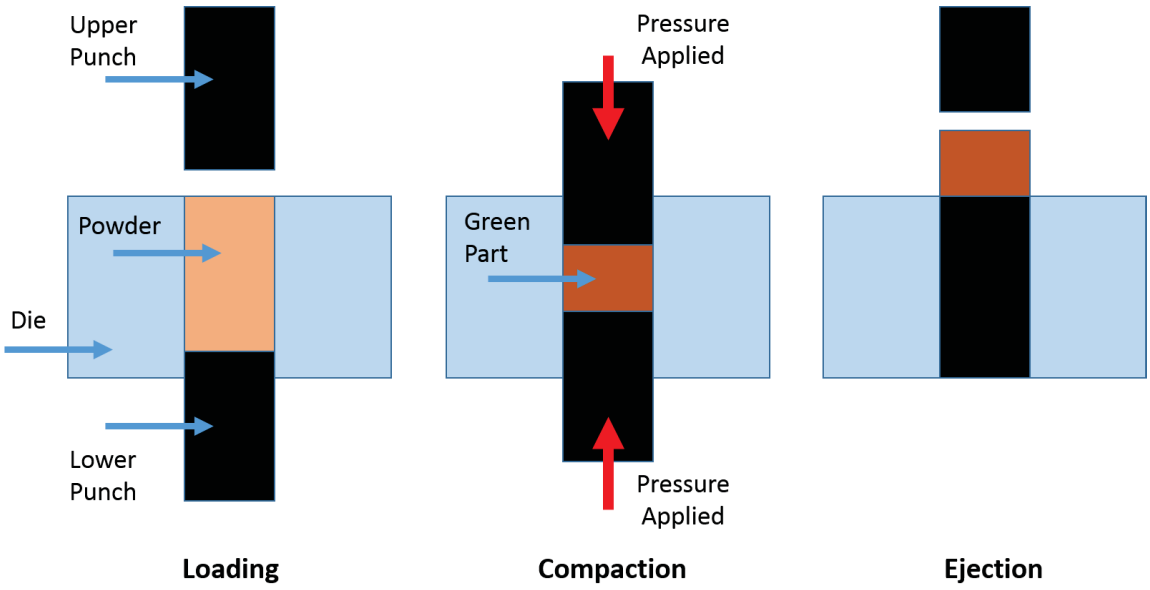

Figure 4: Schematic illustration of the UDC process.

Problems with this production technology emerge when parts with a large cross sectional area are needed and when hard starting particles are utilized. Since the part is only being compacted along one axis, density gradients are formed along the length of the part caused by internal friction between the powder bed and the die wall. If these gradients are pronounced they can lead to sintering-induced distortion so as to compromise the geometry of the sintered product. To minimize this issue, a small amount of wax lubricant is added to the powder mixture to help reduce friction. Even with this addition, a height to diameter ratio under 5:1 must be maintained [28]. When hard particles are present in the powder mix (i.e. fully pre-alloyed powder) particle deformation becomes very challenging. As such, it becomes difficult to produce an interlocking structure that would give the green compact adequate strength for handling.

In CIP technology powders are placed inside a malleable mould that is then sealed and loaded within a pressure chamber filled with a working fluid (Figure 5). The working fluid

is then pressurized so as to compact the powder. The pressure is then released, allowing the user to remove the mold and, in turn, the coherent green compact within it. The main advantage of this process is the fact that the pressure is applied isostatically. Hence, density gradients are minimized. The CIP system can also be very beneficial because large, complex shapes can be formed. However, CIP is disadvantageous in comparison to UDC in that it offers inferior dimensional control as well slower pressing speed which results in a reduced productivity.

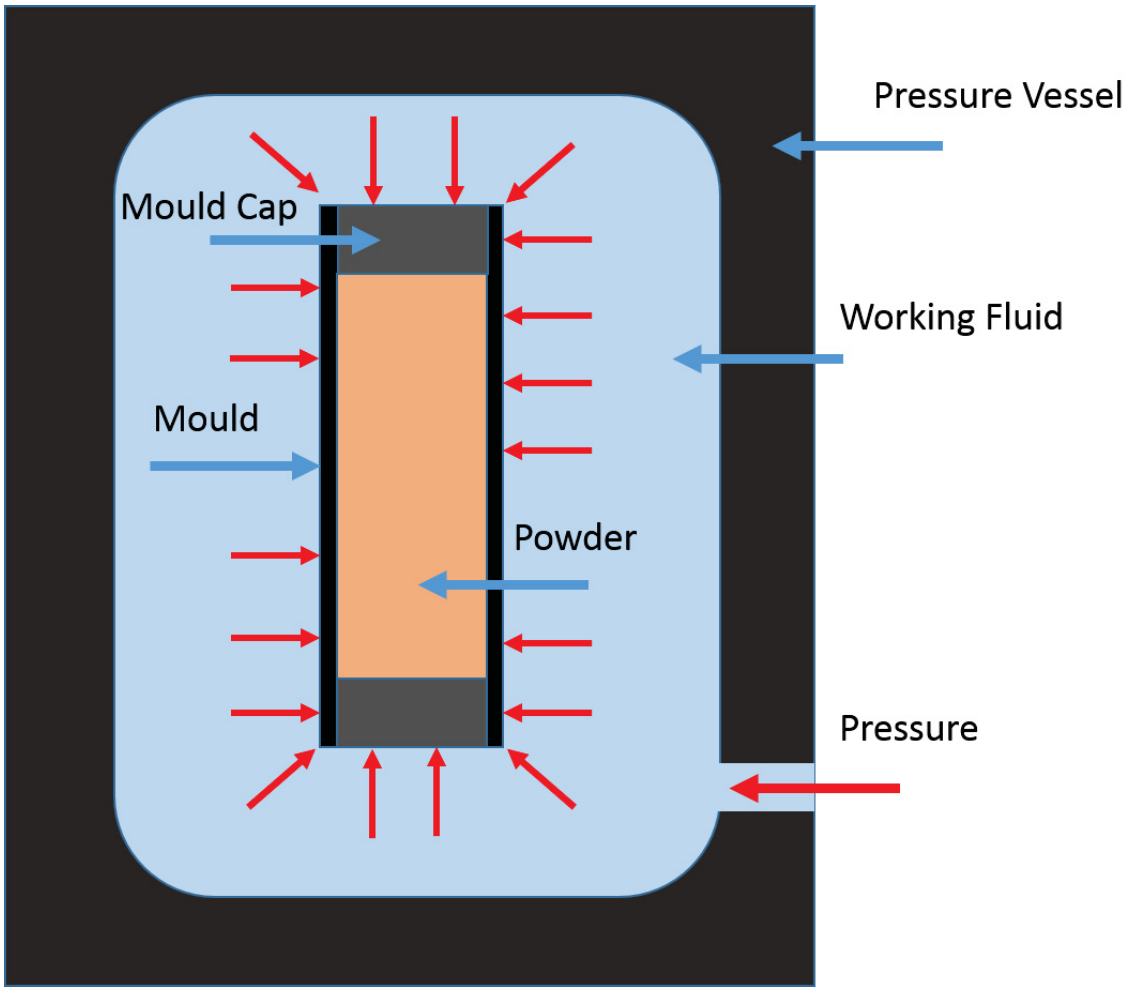

Figure 5: Schematic diagram of a CIP machine.

When considering the compaction pressure to be applied, generally a maximum green density and minimum amount of force is desirable. When looking at the relationship between pressure and green density as seen in Figure 6, a pressure that is in the bulk

densification region is preferable. Once within this region, the lowest possible pressure is favorable, as increasing the pressure further results in diminishing returns with respect to increasing density, yet mandates more costly equipment.

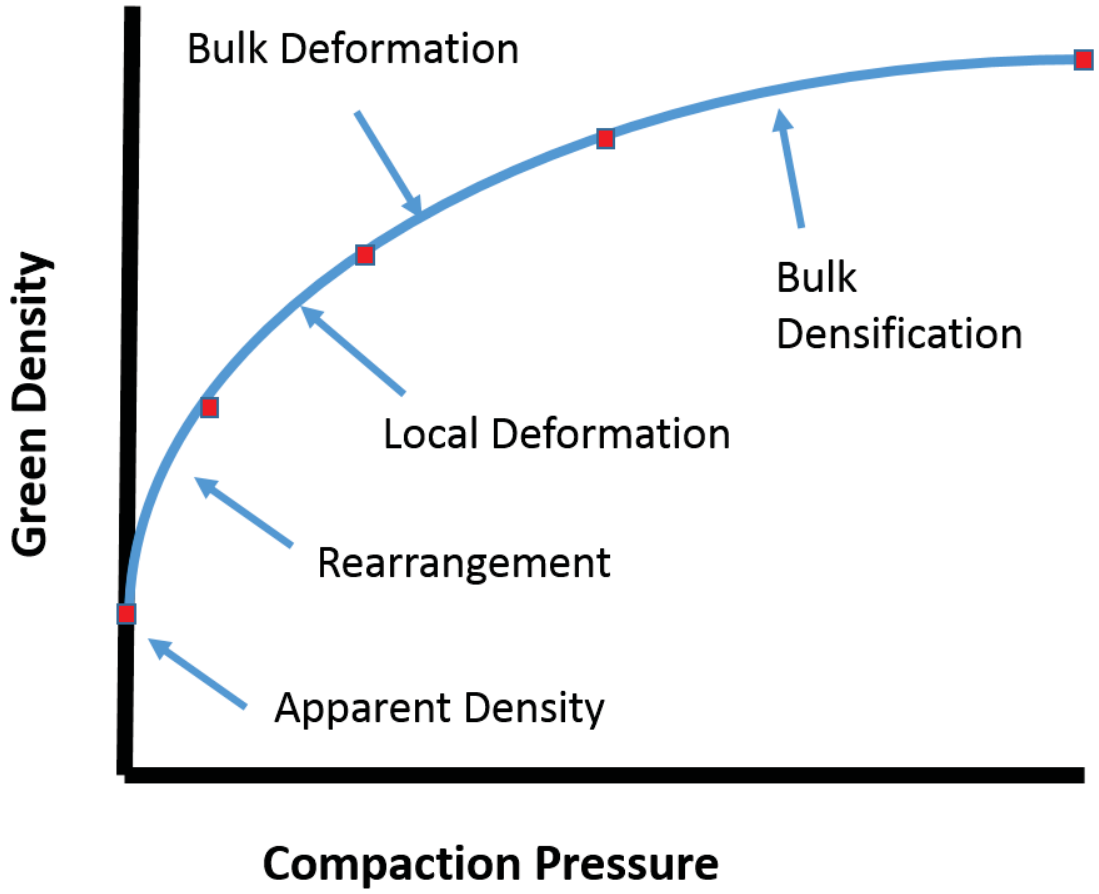

Figure 6: General description of the transition in green density as a function of applied compaction pressure.

Powder size and powder morphology are also characteristics important to compaction. In both cases the apparent density of the powder is altered with changes to these parameters. Packing density or apparent density in a monosized, spherical particle bed is typically 60%. This value is then altered when irregularities are introduced. In general, the more irregular the particle shape, the lower the apparent density of the powder will be. This can cause problems when pressure is applied if the powder particles do not want to rearrange and deform easily. Regarding powder size, a maximum apparent density can be achieved by

having a mixture of both coarse and fine particles. This is because the coarse particles will make up the bulk of the compact, and the fine particles are able to occupy the void areas between them. When a combination of large and small particles are used the apparent density that can be achieved is greater than having only large or small particles alone. Since the apparent density can have a direct impact on the final green density of the part, both of these powder characteristics are of utmost importance and must be considered.

1.2.2 Sintering

Sintering is the stage of production of PM parts where the microstructure and mechanical properties of the part are set. Fundamentally, it is a process of heating the green parts in a controlled atmosphere and temperature for a set amount of time to allow mass transport to occur within the sample. The temperature reached can be below the solidus line (solid state sintering) or a set amount above the solidus line (liquid phase sintering and supersolidus liquid phase sintering) where a controlled amount of liquid is formed within the compact and used to help densify the part. Further refinements may transpire during heat treatment and secondary operations, but if a strong base is not formed during sintering, no amount of secondary processes can remedy the shortfall in metallurgical quality.

Solid state sintering primarily relies on solid state diffusion as a means to densify the compact. Here, individual particles will bond together through necks which are formed when mass is transported between particles and into the region where they come into contact with each other. Because no liquid is formed in this type of sintering, products normally have very good dimensional stability through the sintering process but it is much harder for this process to eliminate porosity from within the sample itself within a reasonable time. The mass transport between particles is said to occur along six principal paths. Each contributes to densification but may act at different rates depending on the temperature. These paths are shown within the two sphere sintering model in Figure 7.

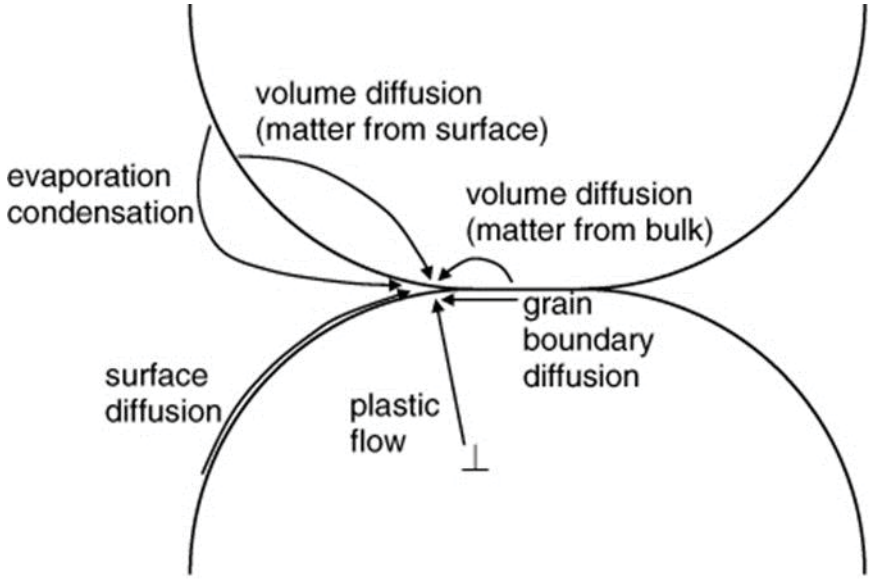

Figure 7: Mass transport mechanisms operative during solid state sintering.

The paths can then be broken up into two major classes of sintering mechanisms, namely surface transport and bulk diffusion. Surface transport mechanisms are evaporation/ condensation, surface diffusion and volume diffusion (matter from the surface) while bulk diffusion mechanisms are plastic flow, grain boundary diffusion and volume diffusion (matter from bulk). Surface transport mechanisms facilitate neck growth by moving mass from one free surface into the neck region whereas with bulk transport processes, the mass that flows into the neck is originally located at the bulk interior. Only bulk transport mechanisms give rise to compact shrinkage [28].

Solid state sintering invokes certain changes to the microstructure that can be broken into three distinct stages. The first (initial stage) is primarily due to surface and grain boundary diffusion and is said to be associated with the onset of neck formation between individual particles. At this state each particle is forming a neck with its contacting neighbors and the first instances of bonding occur. The second or intermediate stage is moreso related to the system trying to reach an equilibrium state. This stage will often establish the properties of the sintered compact and is characterized by densification, grain growth and pore rounding. Once necks are formed between particles in the first stage of sintering, there is a high amount of surface energy remaining in the system. Further diffusion between particles

occurs in an attempt to reduce the surface energy of the compact and thus a gradual reduction and spherodization of pores transpires. Densification in this second stage is attributed mainly to grain boundary and volume diffusion. The last step (so called final stage) of solid state sintering is the reduction in size of isolated spherical pores. The pore shrinking process is mainly attributed to bulk diffusion within the part wherein pores have become isolated on grain boundaries. At the start of this stage the compact is already quite dense. Hence, this stage is often not completed in commercial practice as the practical gains can be limited.

Liquid phase sintering (LPS) is a faster and often more effective sintering technique that relies on the formation of a liquid phase during the sintering process to aid in densification of the green compact. In this process a controlled amount of liquid is formed within the compact which is beneficial for multiple reasons. First, when considering diffusion between the adjacent grains as was the case in solid state sintering, the process is now significantly faster because of the difference in diffusion rates in solids (low) and liquids (high). Second, depending on the sintering atmosphere, the liquid phase will often wet the solid grains and be drawn into the inter-particle voids due to capillary action which invokes significant densification.

To achieve products though LPS there are certain criteria that must be met in order to form a fully dense structure. For one, the liquid phase must be able to spontaneously form a wetting film around the solid phase so that capillary action can engage. Hence, the liquid must have an acute contact angle with the solid particle and is said to be a wetting fluid. A comparison between a wetting fluid, and a non-wetting fluid can be seen in Figure 8.

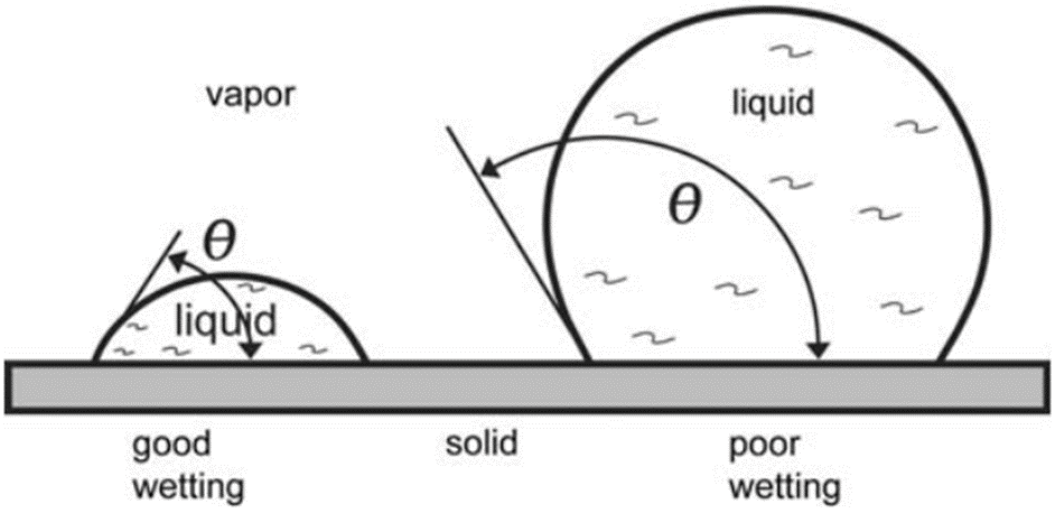

Figure 8: Comparison of good and poor wetting behavior for a liquid [29].

The second and third requirements are that the solid must be soluble in the liquid and that the dissolved solid atoms should have a high diffusivity in the liquid to allow for rapid sintering [28]. The most important requirement however is that the liquid (solute addition) must not be overly soluble in the solid solvent phase. If this condition is not met, the part will not be stable during sintering as transient liquid phase sintering will occur.

Much like solid state sintering, LPS can also be broken into multiple steps. These include solid state heating, rearrangement, solution-reprecipitation and final densification. Within the first step there is no liquid formed and sintering is simply progressing as a solid state process. However, as temperature is increased, a liquid phase is eventually formed, and the rearrangement stage commences. Here, capillary forces draw the liquid into pores which rearranges the solid particles into a more closely packed configuration leading to densification. Once capillary action is exhausted, further densification transpires via solution-reprecipitation. At this point the liquid phase present becomes a carrier for atoms from the solid phase, these atoms which were dissolved in the liquid phase are then reprecipitated onto the larger grains leading to grain coarsening and densification. Finally within the final densification step the liquid further promotes grain shape change which

helps with the removal of pores and produces a fully dense product. A schematic of the microstructural changes occurring during the LPS process can be seen in Figure 9.

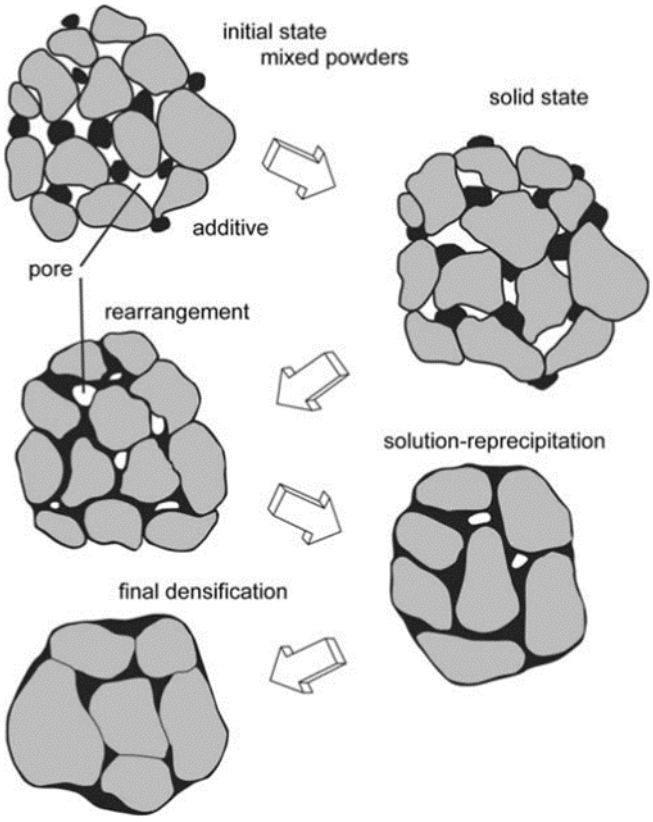

Figure 9: A schematic of the microstructure changes during LPS [29].

It is important to note that densification is not always achieved in an LPS system. If the fluid produced during the process is non wetting this can lead to swelling during the sintering process. This is to say that the final density after sintering can be less than that of the green part. When this is the case some of the liquid formed within the compact may be forced to the surface of the part and solidify as droplets on the surface as seen in Figure 10.

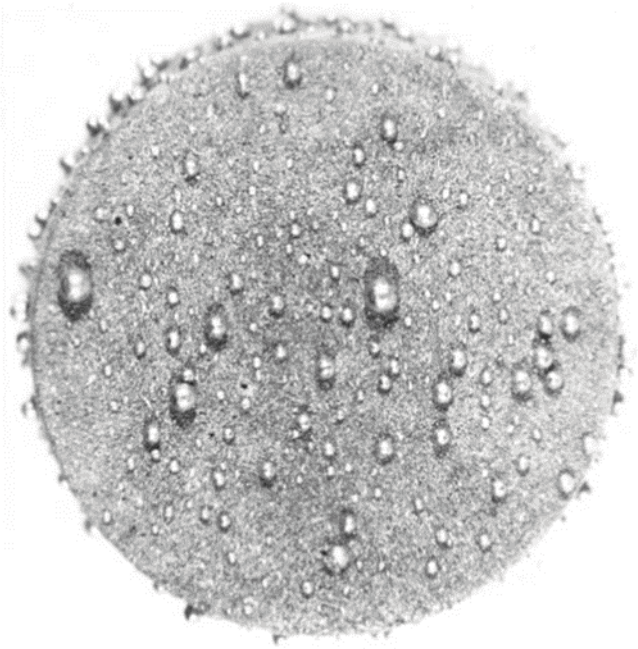

Figure 10: Image of a sample wherein the liquid phase was non-wetting and was thereby forced to the compact surface where it solidified as small spheres [29].

When dealing with the LPS of aluminum alloys temperature and sintering atmosphere are of utmost importance. Because of the relatively low melting point of aluminum, even minor changes in the temperature of the sintering furnace can lead to uncontrolled amounts of liquid formation. This is exasperated by the fact that in many cases the sintering temperature is within 30-50°C of the melting point of aluminum. In terms of the sintering atmosphere, high purity nitrogen is preferential over an inert gas or vacuum. Reportedly, this is because the nitrogen that is trapped within the pores of the sample will be able to react and form aluminum nitride which reduces gas pressure within the pores and concomitantly intensifies capillary action of the liquid phase [30]. With new developments of aluminum PM alloys specifically designed for press and sinter or CIP and sinter processes, it has been shown that small amounts of alloying additions such as tin and magnesium can improve mechanical properties of the sintered products [31]. Tin is specifically used when the sintering atmosphere is nitrogen as it has been shown to retard the rate of nitridation of the aluminum particles. If a nitrogen atmosphere is used alone, then the aluminum nitride that is formed is said to impede the wetting characteristics of the liquid phase formed [32] [33]. Magnesium is also very important because it helps break

down the oxide shell encasing the aluminum particles. Specifically the magnesium will react with this refractory layer and form spinel. This reaction disrupts the continuity of the oxide shell prompting metal to metal contact which thereby allows inter-particle diffusion as well as LPS to occur [34].

Super solidus liquid phase sintering (SSLPS) is another sintering mechanism that requires the production of a liquid within the green compact to aid densification. While the LPS and SSLPS sintering processes have many of the same sintering mechanics, they differ when it comes to the origins of liquid phase. In a traditional LPS system the green powder compact is comprised of a mixture of two or more different powders, generally consisting of base material and then elemental or master alloy additions of the alloying constituent(s). In this system it is the elemental/ master alloy additions which melt and directly produce the liquid phase (see for example the black particles in Figure 9). However, when it comes to SSLPS all powder particles are fully pre-alloyed such that the liquid phase is produced internally within each particle. Eventually this spreads to the particle contacts invoking capillary action on the now semisolid particles [35]. In both cases the part is heated to a region between the solidus and liquidus allowing a controlled amount of liquid formation. With SSLPS, since the liquid is formed within each powder particle, and thus the semisolid particles turn mushy, densification in this system is analogous to viscous flow [36]. The liquid formation can cause the individual particles to fragment into isolated grains, allowing the use of larger initial particles sizes when compared to traditional LPS [37].

1.2.3 Secondary Operations

The term “forging” denotes a family of processes by which plastic deformation of the workpiece is carried out by compressive forces [38]. In general, an initially simple part is placed between two sets of dies and compressed with the goal to produce a part with the desired configuration (size, shape, properties). To attain this desired configuration the forging operation has many different variables that must be considered such as the size/shape of the starting billet, friction at the tooling/die and die/billet interface, nature of deformation zone, equipment, product and environment [39]. Furthermore there are many

different types of forging processes that can be used such as open and closed die forging just to name a few. While a traditional forging process utilizes a cast or wrought billet as the preform, a modern variation implements a sintered preform with the collective concept referred to as “Powder Forging”.

Overall Powder Forging is quite similar to the traditional approach but affords further means of process control such as the density, size and shape of the preform. In general Powder Forging technology can be broken up into two sub sections - powder repressing and upset forging. In the former, material flow is limited and primarily occurs in the pressing direction. In doing so the goal is not to densify the final product but to instill refined dimensional tolerances within the part so as to minimize post-forge machining. Alternatively in upset forging, significant amounts of lateral material flow transpire. Hence, the preform is deformed rather extensively which not only instills part geometry but also densifies and strengthens the material [40]. Due to the fact that the process is associated with a high amount of strain, powder forging is conducted at elevated temperatures to ensure that the material has a lower strength and high ductility [28].

While powder forging is utilized in industry to produce a number of finished parts, it is primarily constrained to ferrous products. Hence, there is relatively little literature available on the powder forging of aluminum alloys, but those that exist have shown promising results. When looking at the work of MacAskill [41], Mann [42], Mosher [43], Bishop [44] and Cooke [45] et al. many of them have reported gains in mechanical strength of the PM-Forged product in comparison to wrought alloys. In general it has been postulated that such gains can be attributed to the presence of fine oxide particulates acting as a strengthening agent within the final product. These oxide particulates are said to be derived from the oxide film present on the aluminum particles which is fractured and dispersed during hot forging.

1.2.4 Uses in Industry

High strength, low weight materials are in demand for both the automotive and aerospace industries. Aluminum-based products are one option that has been exploited extensively in both sectors. For instance, in the automotive industry an average of 394 pounds of aluminum was utilized per light vehicle in 2015. This was up from an average of 212 pounds just 20 years before and 306 pounds 10 years ago. The total consumption is further increased when looking specifically at vehicles such as mini vans, SUV's and trucks. For example, the new 2015 F-150 is the top consumer using 1080 pounds of aluminum per vehicle [46]. Within this push to produce lighter vehicles/aircraft and thus attain improved fuel economy, aluminum PM parts have made some breakthroughs. For instance, Al-Si, Al-Cu-Mg, Al-Zn-Mg-Cu, and Al-Cu-Si-Mg PM alloys are now used for many different automotive applications as they have densities ranging from 2.65 to 2.82g/cc instead of around 7.6g/cc in the case of steel products or 4.43g/cc for Ti-6Al-4V while still meeting strength requirements. Examples include aluminum camshaft-bearing caps, cylinder liners, shock absorber parts and oil pump rotors [47]. As the push for more aluminum in vehicles continues the application of PM aluminum parts will increase as it is ideally suited for the large volume throughput needed with minimum waste [48].

In the aerospace industry the need for high strength 2xxx and 7xxxx series alloys has sparked research into the development of PM alloy equivalents. Up to now the conventionally processed PM materials have had comparable yield strength and hardness to their wrought counterparts but UTS, elongation and fatigue remained inferior. Many of these problems can be attributed to the porosity within the compact and the retained oxygen present from the oxide shell on the powder particles still present after sintering [49][50]. Research into these materials has included work with pre-mixed powders such as Alumix 431D which is a PM equivalent to Al 7075 [41] and also with fully prealloyed powders produced directly from wrought material such as AMPAL 7075 [51].

1.3 Spark Plasma Sintering

Spark Plasma Sintering (SPS) much like conventional UNI or CIP and sinter PM, is a process of compacting powder particles into a near net shape product. The use of the acronym "SPS" is not universally accepted within literature because of the lack of actual information and understanding of what is happening to the sample when it is processed (i.e. scepticism that a spark or even plasma is formed during the process). Hence, the process has been anointed with many different names including electric pulse assisted consolidation (EPAC), pulsed electric current sintering (PECS), current-activated pressure-assisted densification (CAPAD). All of these systems fall under the umbrella category or classification of electric current activated sintering (ECAS), wherein pressure and large electric currents are applied concurrently [52]. Despite the discussion around the naming convention, it has been commonly observed that SPS yields materials with improved physical and mechanical properties [53].

1.3.1 SPS Equipment

The base of an SPS system is much like a uniaxial compaction system wherein the powder is compacted in a uniaxial direction and the die is machined into the shape of the intended part. In this system, a power supply is also attached to the press which allows a current to be passed between the upper and lower rams. When the die and powder assembly is placed between the rams, the electric circuit is completed allowing current to flow. A simple schematic of a typical SPS system can be seen in Figure 11.

To properly allow the flow of current between the upper and lower rams, the die assembly has to be made of an electrically conductive material such as high-purity, high-density graphite [52]. Because of the mechanical limitations of the graphite, relatively low pressures can only be applied. Hence, pressures normally range from 30 – 150 MPa, although higher values are possible. The entire die and ram assembly is normally contained within a vacuum chamber which allows the sintering atmosphere to be controlled

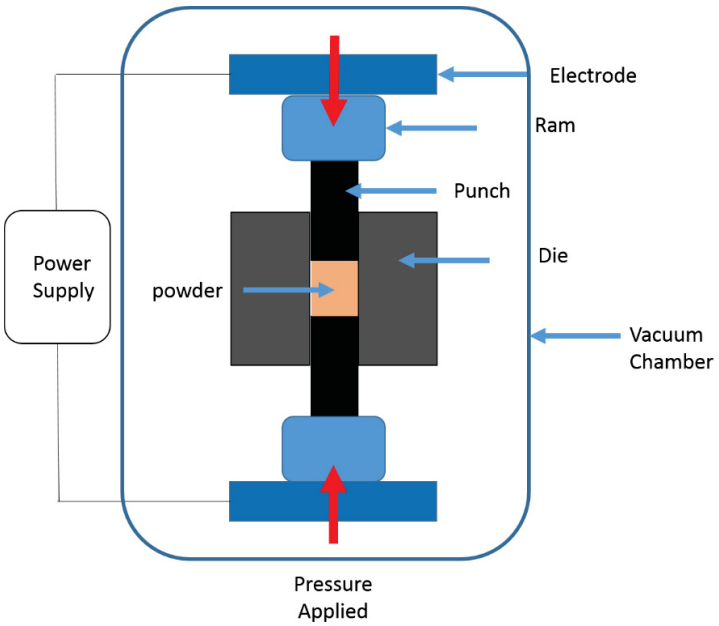

Figure 11: Schematic of a typical SPS system.

The applied current passed between the two rams is normally a pulsed DC wave form and is not controlled directly by the user. Instead, the desired temperature profile is set by the operator and the system will then vary the applied current and voltage to achieve the heating rate and maximum temperature sought. In many systems voltage is on the order of 10's of volts and the current is on the order of 1000's of amps. The use of this type of power supply can be sub categorised as resistance sintering as opposed to electric discharge sintering which uses a capacitor bank to suddenly discharge power through the powder bed [54].

Heating in an SPS system depends on what type of sample is being sintered, namely a conductive vs non-conductive material. In the former, a high-frequency current flows through the die and the green body producing a current skin effect. Eddy currents are also formed within the green body because of the asymmetric distribution of current. The combination of the eddy current, skin effect, graphite die, conductive sample, and direct contact between the die and sample heat is referred to as Joule heating [55]. In the case of non-conductive materials, no current will pass through the green body. Hence, the Joule heating is said to come from the same sources but without the eddy currents produced within the sample.

It has been theorised that during early stages of sintering within the SPS high current densities at the small contact points between powder particles creates a local overheating zone. At this zone the temperature far exceeds the set point of the temperature and causes thermal softening and localized melting at the surface of these particles. This localized overheating is said to support sintering and neck formation between particles [56].

1.3.2 Process Characteristics

Many different process parameters can be manipulated in an SPS apparatus; one of which is the heating rate. Conventional sintering operations such as furnace or hot isostatic press (HIP) sintering are often limited to maximum heating rates up to 50 K/min. Conversely, in a SPS system rates up to 1000 K/min can be achieved with typical values ranging from 100 to 600 K/min. When the heating rate is increased to such an extreme level the time the sample spends at elevated temperatures can be limited such that microstructural coarsening is constrained. In doing so, samples are rapidly heated to a temperature at which grain boundary and volume diffusion are highly active which favours densification [52]. This notion is also supported by modeling work on pure aluminum powder where high heating rates were shown to favor densification over coarsening [57].

The application of pressure in the SPS system is another key driving force behind the densification of the material. Much like in UNI or CIP compaction the applied pressure helps rearrange and deform the powder particles, increasing particle to particle contact. Relatively few studies have focused solely on the effect that pressure alone has on the end product but from the limited work presented some interesting results have been found. First, Garay [52] compiled temperature and pressure information from different papers on multiple materials processed via SPS and found as expected that by increasing the pressure on the samples the density of the final part was increased. It was also noted that specimens produced from pure aluminum powder seemed to increase more with pressure change then those made from ceramic powders (Figure 12).

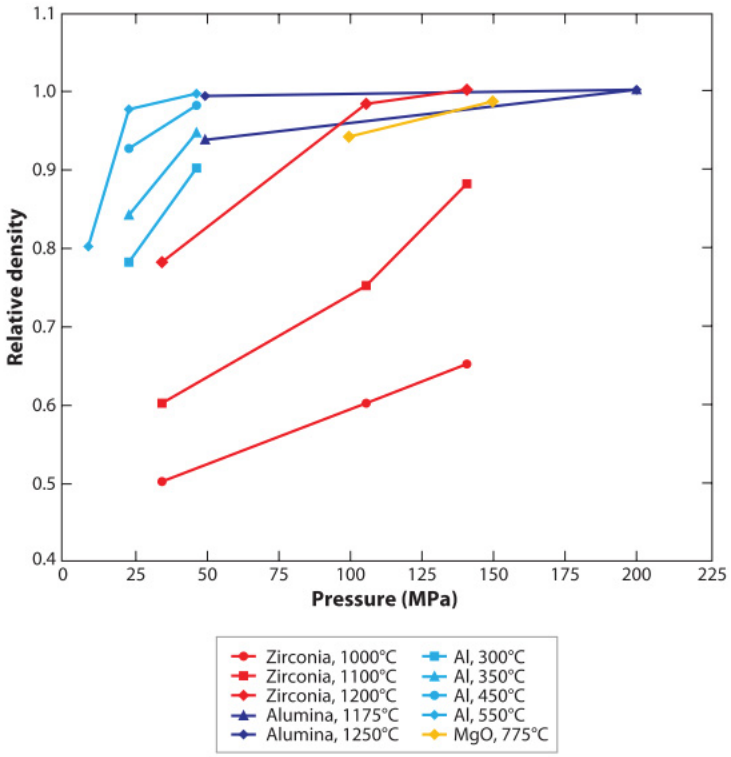

Figure 12: Densification response of various materials when processed through SPS [52].

The effect of pressure was also characterized by Munir et al. in terms of Equation 1 where ρ is the fractional density, B is a term that includes the diffusion coefficient and temperature, g is a geometric constant, γ is the surface energy, x is related to particle size, t is time and P is the applied external pressure [53]. Based on this equation it can be summarized that by increasing pressure there was an increased driving force for sintering which leads to a decrease in the sintering temperature required and reduced grain growth. This conclusion was reinforced through the work of Anselmi-Tamburini et al. which showed that with increasing pressure, the sintering temperature required to achieve 95% of theoretical density was reduced [58].

Equation 1: Driving force for Sintering

$$\frac{d\rho}{(1-\rho)dt} = B\left(\frac{g\gamma}{x} + P\right)$$

The effects of the applied current have been studied extensively. This is normally supplied as a pulsating DC current with a time on/off on the order of milliseconds. Its influence on mass transport within the sample was assessed by varying the current density applied to layered assemblies of materials and then inspecting the growth of the intermetallic phases formed between them. In a group of papers published by Bertonino et al. current density was shown to play a major factor in the growth of intermetallics in the Al-Au and Ni-Ti systems [59][60][61] as noted in Figure 13. This was attributed to electron wind or electro-migration [59] and increases in point defect concentrations [62].

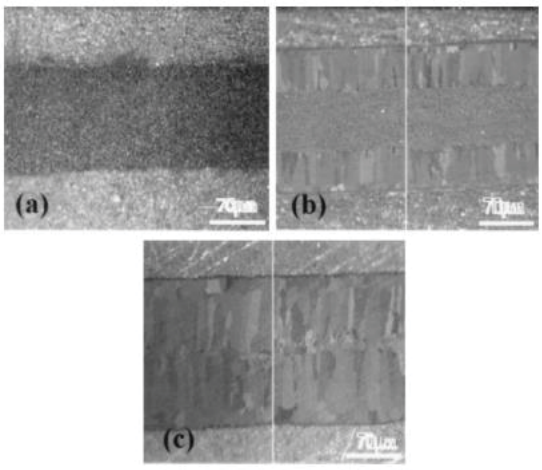

Figure 13: Optical micrographs showing intermetallic phase formation under different levels of applied current density. (a) No current, (b) intermediate, and (c) high current density [59].

In a three part study by Chen et al. focusing on the effects of pulsing and current on the reactivity of the material within the SPS it was shown that the direction of electron flow and the pulse pattern had no effect on the thickness of intermetallic layers formed within their Mo-Si-Mo samples [63]. It was also shown that the diffusion kinetics of the reaction were increased with the application of current. However, since the activation energy was unchanged, the reaction mechanisms for diffusion were deemed unaltered [64] and were attributed to an increase in mass transport mechanisms previously mentioned.

1.3.3 SPS of Aluminum-Based Powders

Using current to activate sintering of aluminum powders is not a new idea as the first attempt at this was completed in 1977 by Kol'chinskii et al. [65]. Since then a sizable body of work has been completed. Xie et al. have focused on the bonding of aluminum particles in the SPS and the effect of the surface oxide films present [66][67][68][69][70]. The group found that within the sintered aluminum compacts there was combinations of metal/oxide/metal bonds and metal/metal bonds. In the first, the metal particles remained separated by the oxide shell on the particles, while the latter represented a strong sintering response where the oxide shell was disrupted. It was shown that breakup of the oxide shell was dependant on pressure and temperature and that a rise in the loading pressure at elevated temperature facilitated the effect. This concept was further investigated by Zadra et al. [71] whom effectively observed the same result. Another study on trace impurities such as oxygen and hydrogen showed that the concentrations of both species were reduced as a result of SPS [72][73]. Furthermore, the response of a broadening range of alloy chemistries to SPS has now been studied. Some are simple chemistries such commercially pure aluminum while others are complex members from the 2xxx [74][51], 5xxxx [75][76], and 7xxx [77][78] series. Unfortunately, a systematic shortfall in many of these works is a lack of data on the mechanical properties (tensile, fatigue, etc.) of the consolidated products.

CHAPTER 2. RESEARCH OBJECTIVES

The central objective of this research was to perform a fundamental assessment of the sintering response of a gas atomized aerospace grade aluminum 7055 powder. Both a CIP-Sinter-Forge and SPS-Forge approach were investigated with a key interest in determining the process parameters that produce a product with the highest mechanical properties. In CIP-Sinter-Forge processing key variables included; sintering temperature, particle size, and forging temperature. In the SPS-Forge approach, experimental parameters stressed sintering temperature, sintering time and the point at which pressure was applied to the system. In both cases the final product was compared against its wrought counterpart in terms of mechanical properties.

CHAPTER 3. CONSOLIDATION OF AEROSPACE GRADE ALUMINUM 7055 POWDER VIA SINTER-FORGE PROCESSING

N.P. Kraus and D.P. Bishop
Dalhousie University
Department of Process Engineering and Applied Science
1360 Barrington St., Halifax, Nova Scotia, Canada, B3J 1Z1

R.L. Hexemer Jr. and I.W. Donaldson
GKN Sinter Metals LLC
2200 N. Opdyke Road, Auburn Hills, USA, 48326

Status: Published Conference Proceedings, 2016 International Conference on Powder Metallurgy & Particulate Materials – POWDERMET 2016 in Boston USA, on June 7, 2016. ***Winner "Howard I. Sanderow Most Outstanding Technical Paper" Award***

The following experimental procedures, results and discussions were completed by N.P. Kraus, with reviewer and editorial roles played by the co-authors.

Abstract

The objective of this research was to assess the response of gas atomized 7055 powder to a sinter-forge style of powder metallurgy processing. In meeting this objective the powder was processed through a three-stage sequence of cold isostatic pressing, liquid phase sintering, and rotary forging. Core variables included average particle size, the effects of admixed sintering activators (Mg, Sn), and forging temperature. Admixed additions facilitated modest gains in as-sintered density but compromised forging response. The removal of fines (<45μm) from the starting powder invoked positive gains in forging behaviour and the ability to produce a defect-free product. Once heat treated to the T76 state, optimal sinter-forge products attained near full theoretical density as well as hardness and tensile properties that closely replicated those of the wrought counterpart.

3.1 Introduction

When considering the commercial use of aluminum within the transportation industry, significant volumes of this metal are required in the automotive sector. For instance, the current average amount of aluminum used per light vehicle in 2015 was 179 kg (394 lbs). This weight significantly increases when looking at larger light vehicles given that 491 kg (1080 lbs) are utilized in the 2015 Ford F-150 truck [46]. Among the many metal forming operations involved in the fabrication of components that add up to these net weights,

aluminum powder metallurgy (PM) is playing an increasingly important role in the fabrication of numerous items such as camshaft-bearing caps, shock absorber parts, and oil pump rotors [47]. Currently, these components are processed through die compaction-sinter-size manufacturing operations. This is largely driven by the fact that this technology is conducive to the near-net shape fabrication of geometrically complex components in high annual volumes.

When producing aluminum PM parts for the aerospace sector the need for high volume throughput and net shape become less imperative, as functional performance takes a leading role (mechanical properties, microstructural homogeneity, reduced levels of impurities, etc.) along with the ability to produce parts of a size that is far beyond the capabilities of die compaction. Hence, the associated raw materials and processing sequence must be adjusted accordingly. One scenario that has the potential to meet these requirements is that whereby fully prealloyed aluminum powder is processed by cold isostatic pressing (CIP) coupled with sintering and hot forging (hereafter denoted as "CIP-Sinter-Forge"). Utilizing prealloyed aluminum powder as the starting raw material is advantageous as it offers a capacity to achieve a refined and homogenous microstructure. CIP desirable as it requires no admixed lubricant, produces large parts with uniform green density [79], and is amenable to the processing of prealloyed aluminum powders [80]. Likewise, the tandem of sinter-forge is also beneficial as it is known to instill advantageous tensile and fatigue gains within the finished aluminum PM products [41][81][42].

Numerous aluminum PM alloys have been commissioned for use within the aforementioned sectors. However, most are based on counterparts to traditional wrought alloys within the 2xxx or 7xxx series. Examples include 2014 [82], 2024 [42][83], 2618[81], and 7075 [41]. Indeed, many other alloy chemistries have yet to be considered within the domain of PM; in particular, those based on more modern wrought alloy formulations. One example is alloy 7055 (Al-8Zn-2.1Mg-2.3Cu-0.2Zr) which was specifically designed for aerospace applications with demanding compressive strength requirements. The open literature indicates that this alloy has yet to be studied within any

variant of press-sinter PM technology. Hence, the objective of this research was to assess the response of 7055 powder as processed through a CIP-Sinter-Forge sequence of operations.

3.2 Materials

The aluminum alloy of interest in this study was 7055. It was investigated in two different forms - one being that of a wrought plate with the second that of a fully prealloyed powder (hereafter denoted as "PA7055"). The later was produced through gas atomization of the as-received material at Ecka Granules (Furth, Germany). The chemistry of the wrought and PA7055 materials were verified through inductively coupled plasma optical emission spectrometry (ICP-OES). As seen in Table 5 the chemistries of both the wrought and powdered alloys were well aligned with the accepted chemistry for 7055 as specified by the Aluminum Association. Two different particle size ranges of PA7055 powder were utilized in the production of consolidated products. One was the as-received powder which had a D_{50} of 85μm. The second was a variant screened to remove particles smaller than 45μm thereby yielding a product with a D_{50} of 149μm. These two powder sizes will be referred to as "As-Received" and ">45μm" from this point forward. Complete particle size distributions for each cut as attained through laser light scattering are shown in Figure 14.

Table 5: Measured compositions of the raw materials in comparison to the chemical specifications for aluminum alloy 7055. All values in weight % with the exception of oxygen which is reported in ppm.

Material	**Chemistry**	**Al**	**Zn**	**Mg**	**Cu**	**Zr**	**Fe**	**O (ppm)**
7055	Spec.	Bal	7.6 – 8.4	1.8 – 2.3	2.0 – 2.6	0.08 – 0.25	0.15	N/A
Plate 7055	Measured	Bal	7.97	1.85	2.12	0.16	0.07	40
PA7055	Measured	Bal	8.06	2.10	2.39	0.11	0.05	480

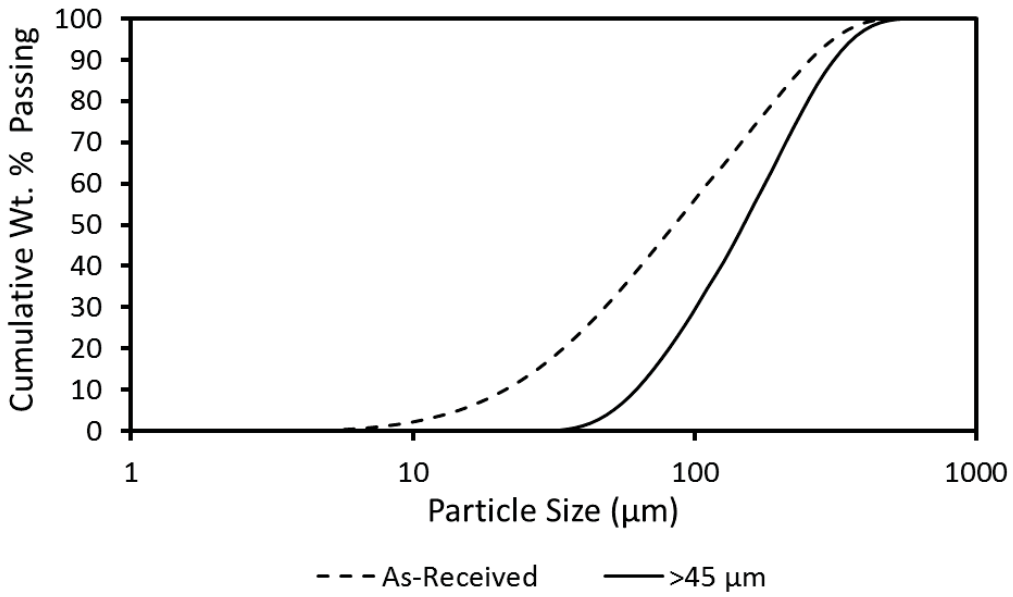

Figure 14: Particle size distributions for the two cuts of PA7055 powder studied.

3.3 Experimental Techniques

Powders were initially consolidated by means of a model LCIP 42260 Cold Isostatic Press (CIP) manufactured by Quintus Technologies Inc. (formerly Avure Technologies). This particular model had a peak pressure of 414 MPa (60 ksi). In using this apparatus, powder was first poured into rubber moulds that were sealed with a rubber stopper and hose clamp. Each mold was then vacuum sealed in a mylar bag. Specimens were then loaded into the CIP and pressed at the desired pressure. Green compacts were subsequently removed from the moulds and sintered either in a laboratory furnace or within industrial furnaces at GKN Sinter Metals at temperatures ranging from 520 to 640°C. The former involved processing under flowing high purity nitrogen in a three-zone tube furnace equipped with a stainless steel tubular retort. The latter were sintered in a continuous mesh belt furnace also operated with a flowing atmosphere of high purity nitrogen. The thermal cycle in both cases targeted a 20 min hold at 400°C followed by a 20 min hold at the particular sintering temperature of interest followed by furnace cooling within water-jacketed sections of the furnaces. Sintered slugs were machined into cylindrical specimens with a diameter of 12 mm. These were then heated to the required hot forging temperature (450, 470 or 490°C) and allowed to soak for 1 hour before processing in a rotary swaging machine. Forging was executed in a series of 3 progressively smaller die sets with the billets reheated for 20 min between

consecutive runs. A net reduction in the cross sectional area of ~50% was ultimately realized. Forged products were then heat treated to the T76 condition (solutionized at 472 ± 5°C for 90 min, quenched, and aged for 5 hours at 121°C followed by 7 hours at 160°C).

Characterization of the materials involved a number of techniques. Apparent density was measured using an Arnold meter in accordance with MPIF standard 48. Powder flow was measured using a Carney style funnel filled with 25 grams of powder. Green and sintered density was measured using standard Archimedes principals combined with oil infiltration and water immersion. Microscopy samples were initially mounted using a cold mount resin, then subsequently polished through a series of grit papers and diamond polishing steps. Those studied in the SEM (Hitachi S-4700) were carbon coated after final polishing and then examined under an accelerating voltage of 20kV and a beam current of 15 mA. The SEM was equipped with an Oxford Instruments X-Max detector for chemical analyses of microstructural constituents via energy dispersive spectroscopy (EDS) and a secondary detector for texture analyses via electron back-scatter diffraction (EBSD). Hardness was measured in the HRB scale using a Wilson Hardness Rockwell 2000 machine. Tensile testing was performed with an Instron Model 5594-200HVL load frame equipped with a 50kN load cell and an Epsilon model 3542-025M-050-ST extensometer.

3.4 Results and Discussion

3.4.1 Compaction Response of PA7055

Research on powder compaction began with basic testing on the fundamental attributes of flow rate and apparent density. Per the data of Table 6, when fine particles were removed through screening in the >45 μm powder, the flow rate increased while the apparent density of the powder was reduced.

Table 6: Data on the basic attributes of PA7055 powders.

Powder	Flow Rate (g/s)	Apparent Density (g/cc)
As-Received	3.2	1.75
>45μm	4.9	1.57

Compressibility curves for the powder cuts of interest are shown in Figure 15. From this testing a compaction pressure of 400 MPa was found to have the highest density in both instances and that samples produced with the As-Received powder show a higher green density than those produced with the fines removed (>45μm). This trend coincided with the data seen in Table 6 showing that the

As-Received powder which has a higher apparent density also had a higher green density as expected. While the green density of the As-Received powder was improved, all values were still relatively low owing to the fact that the powder was of a fully pre-alloyed nature. Furthermore the As-Received densification trend of PA7055 was almost identical to values presented by Chua et al. on the CIP behaviour of another 7xxx series fully prealloyed powder with a similar chemistry [84]. While the implementation of higher CIP pressures was desirable, this could not be studied due to the capacity limitation of the apparatus. Hence, all samples for sintering studies were CIPed at 400 MPa.

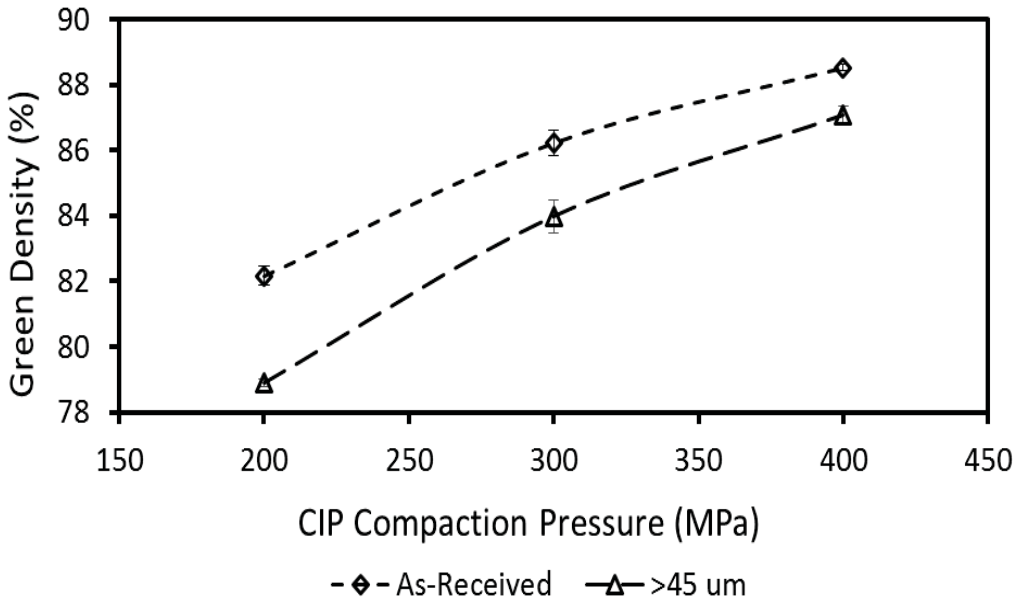

Figure 15: Compressibility curves for the two cuts of PA7055 powder studied.

3.4.2 Sintering Response of PA7055

3.4.2.1 As-Received Powder

To first assess the sintering response of the As-Received PA7055 powder it was important to establish a baseline data set revealing the transition in sintered density as a function of sintering temperature (Figure 16). Per these data, a clear trend was observed whereby as sintering temperature increased, sinter density did so as well but only up to a temperature of ~560°C. Density then remained static until 600°C after which the trend then reversed and a gradual reduction in density ensued. The peak density was ~96.5% of full theoretical which represented a sizable gain over the starting green density (88%). Based on this information a sintering temperature of 580°C was chosen as an appropriate value. An image of the corresponding sintered microstructure is given in Figure 17. Inter-particle bonding was apparent although the general extent of which remained somewhat marginal given that the spherical morphology of the starting powder remained apparent. Furthermore, the residual porosity was rather abundant and largely non-spherodized. Hence, while the PA7055 powder had clearly sintered, the general sinter quality remained somewhat modest.

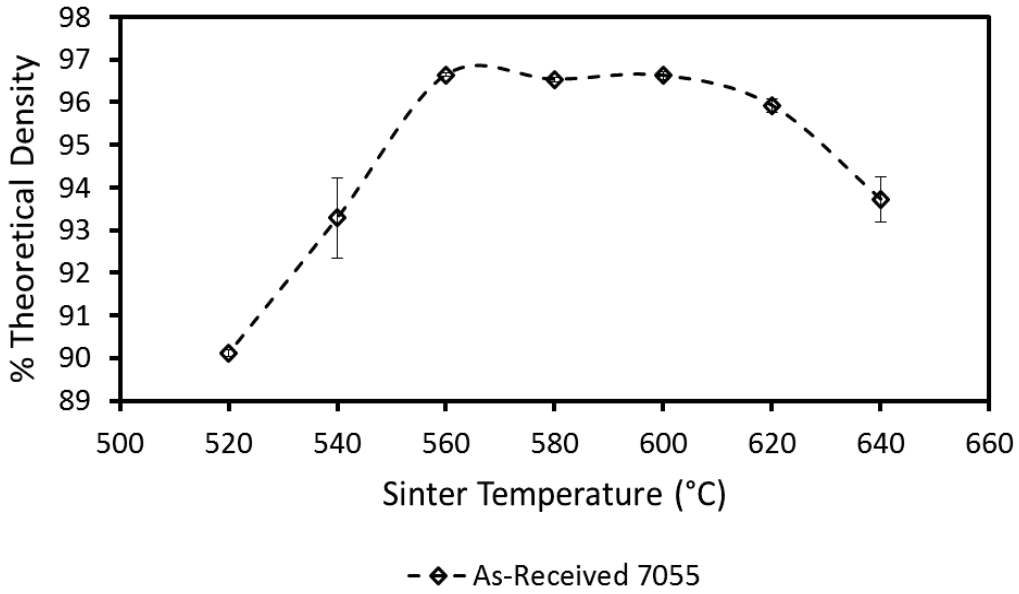

Figure 16: Baseline sintering response of PA7055 (As-received powder; all samples CIPed at 400 MPa).

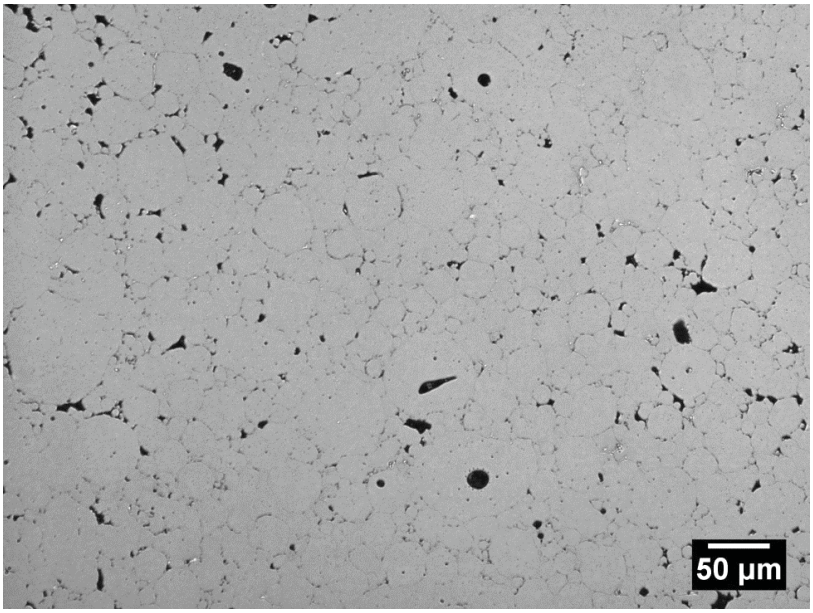

Figure 17: Microstructure of PA7055 (As-Received) after sintering at 580°C.

To further reinforce the notion that a sintering temperature of 580°C was appropriate, EDS analyses were completed on select samples to quantify the α-aluminum grain chemistries. When looking at key examples of the data generated (Table 7) it was clear that the higher sintering temperature yielded a product with lower concentrations of all alloying additions within the α-aluminum grains. This transition was believed to be a direct consequence of super solidus liquid phase sintering (SSLPS). In this sense, the solidus temperature for alloy 7055 is known to be 554±5°C as found by DSC analyses. This ensured that both of the samples assessed in Table 7 were sintered in accordance with SSLPS. It is common knowledge that the fraction of liquid phase present as well as the net concentrations of alloying additions within this liquid increase proportionately with rising SSLPS temperature. When these semi-solid compacts are then cooled from the sintering temperature in an accelerated manner, the constituents of the liquid phase have insufficient time to diffuse back into the adjacent α-aluminum grains. This causes the solute-enriched liquid to solidify into an inter-granular feature within the microstructure thereby depriving the grains of critical elements needed to maximize precipitation strengthening within the sintered product. The data of Table 7 are supportive of this concept and stress the need to utilize the lowest sintering temperature possible.

Table 7: Comparison of the α-aluminum grain chemistries (wt. %) within specimens of PA7055 sintered at 580 and 640°C. As-Received PA7055 powder.

Sintering Temperature	Element				
	Al	Zn	Mg	Cu	Zr
580°C	Bal.	8.26	1.49	2.60	0.14
640°C	Bal.	7.46	1.35	1.81	0.19

3.4.2.2 Effects of Sintering Aids

As the general sintering response of the PA7055 powder was seemingly less than ideal, it was appropriate to consider the effects of metallic sintering aids. In particular, the addition of minor amounts of elemental magnesium and tin powders were explored as both can have a positive effect on the sintering response of aluminum alloys [31]. Considering magnesium, this addition enhances sinterability by disrupting the oxide shell on powder particles via a chemical reaction. Specifically, the magnesium purportedly reacts with aluminum oxide and forms spinel thereby rupturing the continuity of the refractory shell and allowing for the development of metallic Al-Al bonding instead of low strength Al-Oxide-Al bonding [34]. The effects of varying amounts of admixed elemental magnesium additions on sintered density are shown in Figure 18. The general trends for each concentration considered were quite similar to the behaviour noted for the base powder alone (Figure 16). In this sense, density rose at first with increasing sintering temperature, plateaued and then declined at the higher temperatures >600°C. Likewise, the most appropriate sintering temperature was again 580°C in all instances. The highest density was achieved with the lowest amount of admixed magnesium (0.1%) but this value was effectively identical to that achieved in the base powder alone. Higher concentrations of magnesium brought about a progressive reduction in densification such that the density of the system prepared with 0.5% magnesium fell to 96.4%. This deteriorated sintering response was also evident in the sintered microstructures as a higher concentration of internal porosity was evident as was a generally inferior sinter quality. Based on this information, admixed magnesium was ruled out as a potential sintering aid.

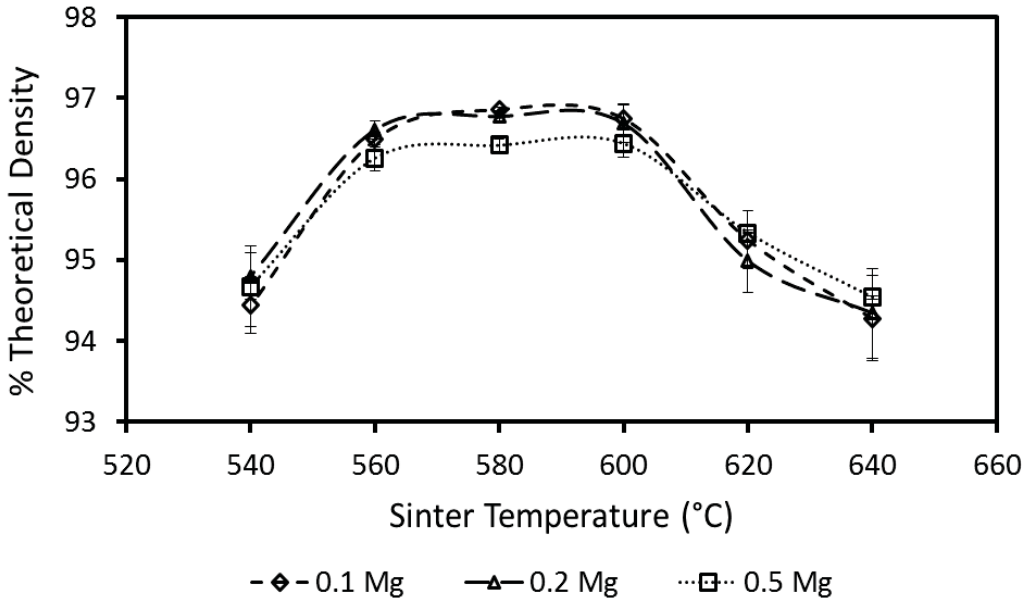

Figure 18: Effects of admixed magnesium on the sintering behaviour of As-Received PA7055 powder.

Regarding tin, the addition of this element is used in conjunction with a nitrogen sintering atmosphere because it has been shown to subdue the rate of nitridation of the aluminum particles [33]. Nitrogen is of key importance during the sintering of aluminum compacts because of its ability to aid densification. Here, nitrogen present within the pore reacts with the aluminum particles forming an outer shell of aluminum nitride. This reaction favorably alters the wetting characteristics between the liquid and the surface of the Al particles while simultaneously lowering the internal pore pressure so as to induce pore filling [32]. While nitridation in this manner is favorable, the reaction can also have a negative impact if left to occur in an uncontrolled fashion given that excessive amounts of aluminum nitride can form so as to produce a rigid network which can restrict shrinkage within the sintering product. By supressing the rate of nitridation with tin, a more desirable balance between the positive effect of pore filling and the negative impact of reduced sintered density can then be realized.

The sintering response of the PA7055 powder as modified with differing amounts of admixed tin is shown in Figure 19. When comparing these results to those of the baseline system seen in Figure 16, tin imparted an increase in the sinter density across all

temperatures. Consistent with prior findings, a sintering temperature of 580°C again appeared to be an appropriate processing condition for the tin-modified mixtures. Unlike the density trends seen with only the base powder (Figure 16) and with admixed magnesium (Figure 18) a sharp drop in sintered density was not seen at sintering temperatures above 600°C. At a sintering temperature of 580°C a peak density of 97.7% was attained for both blend chemistries representing a tangible increase of 1.2% over tin-free specimens sintered under identical conditions. The benefits of tin addition were also apparent in the sintered microstructures as shown in Figure 20. When comparing this image to that of Figure 17, less porosity and particle boundaries were observed in this sample. Combining this information with that attained from the density vs. temperature plots it was concluded that tin additions had a positive response on the sintering of the alloy. As both concentrations of tin offered comparable gains, the lower level of 0.2% was utilized in all subsequent processing so as to minimize the deviance from the chemical specifications for alloy 7055. A lower amount of tin was also desirable because of the potentially negative impact that it may have on the heat treatment response of the alloy. In this sense, it is known from prior studies that tin will consume magnesium to form the thermodynamically stable phase Mg_2Sn. This invariably reduces the amount magnesium available for precipitation hardening via the η ($MgZn_2$)-based series of reactions, thereby lowering the concentration of precipitates, and in turn, the mechanical properties of the final product.

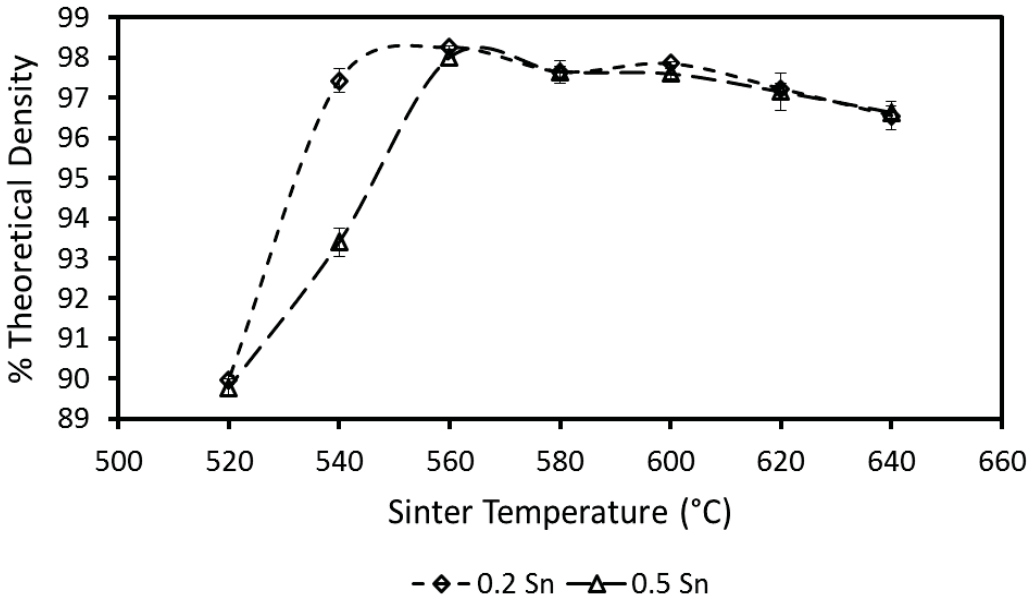

Figure 19: Effects of admixed tin additions on the sintering behaviour of As-Received PA7055 powder.

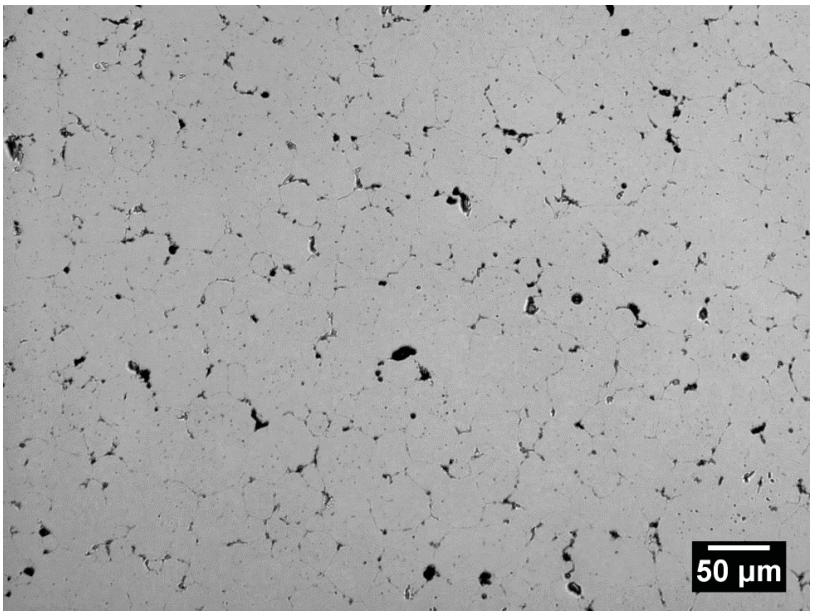

Figure 20: Microstructure of As-Received PA7055 powder admixed with 0.5% tin and sintered at 580°C.

3.4.2.3 Effects of Particle Size

In an effort to further enhance the sintering response of PA7055 powder the effects of particle size were investigated in conjunction with the absence/presence of admixed tin. Here, additional tests were completed wherein the base powder was switched to the coarser >45μm cut. Starting with sintered density (Table 8) it was noted that a lower overall density was achieved in these products when compared to their As-Received blend counterparts. This reduction in sinter density by approximately 1.5% can be directly attributed to the lower green density of >45μm powder. While the sintered density of the >45μm samples was lower, retained porosity within the samples was still rounded in nature. Based on the extent of pore rounding and the fact that retained porosity was situated mostly on grain boundaries, samples underwent a full sintering cycle.

Table 8: Effect of powder cut and admixed tin on the density of samples sintered at 580°C.

Powder Cut	**Tin Content** (wt. %)	**Sintered Density** (% Theoretical)
As-Received	0.0	96.5
As-Received	0.2	97.7
>45μm	0.0	94.9
>45μm	0.2	96.2

3.4.3 Industrial Sintering Response

At this point in the study a transition was made whereby all subsequent sintering was completed within industrial furnaces utilized in high volume aluminum PM parts production. Here, the objective was to determine if key laboratory findings were reproducible in this setting. Data on sintered densities are shown in Table 9. When looking at these values, the attenuation of a moderately higher density with the addition of tin prevailed thereby confirming laboratory findings. In general, all density values realized within the two sintering environments were in close agreement.

Exemplary microstructures of industrially sintered bars are shown in Figure 21. These micrographs were highly comparable to the microstructures previously observed in lab-sintered bars in terms of the nature/distribution of residual porosity and the general extent

of inter-particle bonding. Microstructural consistency was further accentuated through EDS analyses whereby strong agreement in the α-aluminum grain chemistries was noted between the bars sintered industrially (Table 10) and on a lab scale (Table 7). This boded well for eventual heat treatment of the industrial products given that the majority of the solute elements were not trapped as a potentially insoluble intergranular feature and were therefore available for precipitation hardening mechanisms. Alternatively tin was added to the powder as an elemental addition and thus was not present within the α-aluminum grain matrix and was instead located largely at grain boundaries. Overall, it was concluded that there was reasonable agreement between lab and industrial products within each of the attributes considered. Accordingly, industrially sintered bars were then implemented as the substrate materials for the final phase of research dedicated to hot forging and heat treatment.

Table 9: Densities for specimens of PA7055 sintered in an industrial production furnace. All materials originally CIPed at 400 MPa.

Powder Cut	**Tin Content** (wt. %)	**Sinter Density** (% Theoretical)
As-Received	0.0	96.1
As-Received	0.2	96.7
>45μm	0.0	95.4
>45μm	0.2	96.7

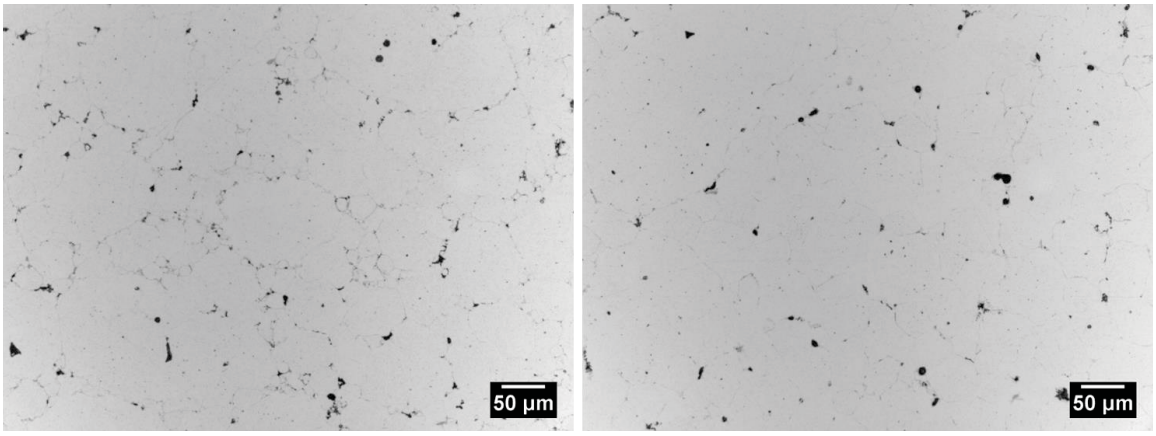

(a) (b)

Figure 21: Microstructures observed in industrially sintered specimens of (a) As-Received and (b) >45 µm PA7055 powder. Both materials originally CIPed at 400 MPa and contained 0.2% tin.

Table 10: Comparison of the average α-aluminum grain chemistries (wt. %) within industrially sintered specimens of As-Received and >45µm PA7055 prepared with 0.2 wt. % admixed tin.

Particle Size	Element					
	Al	Zn	Mg	Cu	Zr	Sn
As-Received	Bal.	8.54	1.74	2.25	0.16	0.03
>45µm	Bal.	8.23	1.75	2.21	0.18	0.03

3.4.4 Hot Forging of Sintered Preforms

To improve the metallurgical attributes of industrially sintered bars a hot forging process was implemented so as to collapse residual porosity and simultaneously disrupt the network of residual oxides and nitrides generated in-situ during sintering. Sintered bars of each material discussed in Table 9 were fabricated for this purpose. In the initial stage of forging trials, all were pre-heated to a fixed temperature of 470°C (i.e. the solutionizing temperature for heat treatment) and hot forged. Both materials produced from the As-received PA7055 powder cracked extensively irrespective of the absence or presence of tin. In some cases the starting billet ruptured in numerous, small sections while in others, the final specimen was largely intact but was riddled with an abundance of readily visible cracks that propagated transverse to the direction of material flow. Conversely, sound, defect-free forged products were produced when the coarser cut of powder was employed as the base material. Micrographs depicting these differences are shown in Figure 22. Fractures had

a clear tendency to follow an inter-particle path. Hence, it was postulated that these had either stemmed from pre-existing green cracks or that the inter-particle bonds had failed to develop sufficently during sintering. The latter was likely exasperated by the fact that the as-received powder would have had a proportionately higher oxide content on a unit volume basis when compared to the >45µm cut, thereby presenting a greater impediment to sintering. Given the friable nature of the billets sourced from As-Received powder, forging research on these particular materials was discontinued at this point.

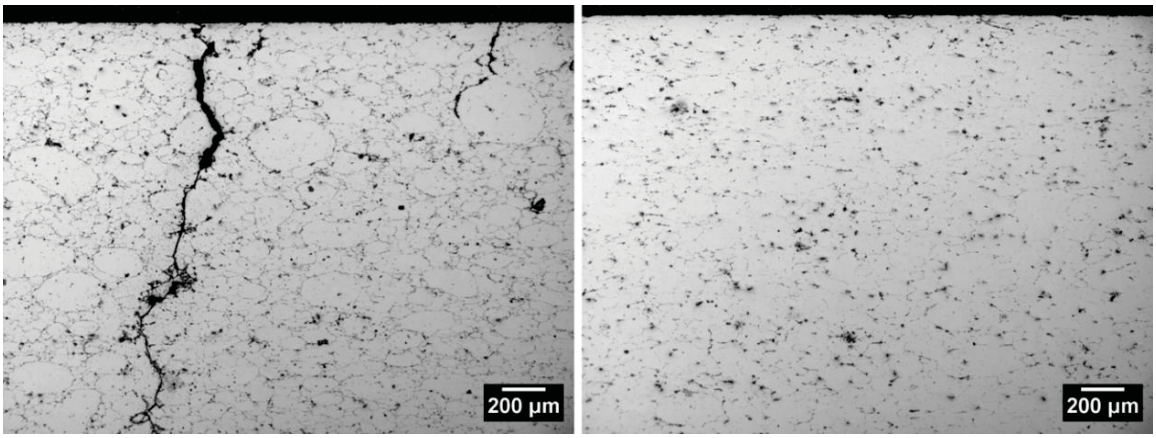

(a) (b)

Figure 22: Comparison of the as-forged microstructures observed within samples prepared from (a) As-Received and (b) >45µm powders. Both materials contained 0.2 wt. % tin and were forged at 470°C.

Data on the densities of successfully forged samples of PA7055 are shown in Figure 23. Both samples were responsive to forging from this perpsective as near full theoretcial density was realized in each instance. This occurred irrespective of the absence/presence of admixed tin thereby confirming that this modification did not play a significant role in the densification instilled by forging.

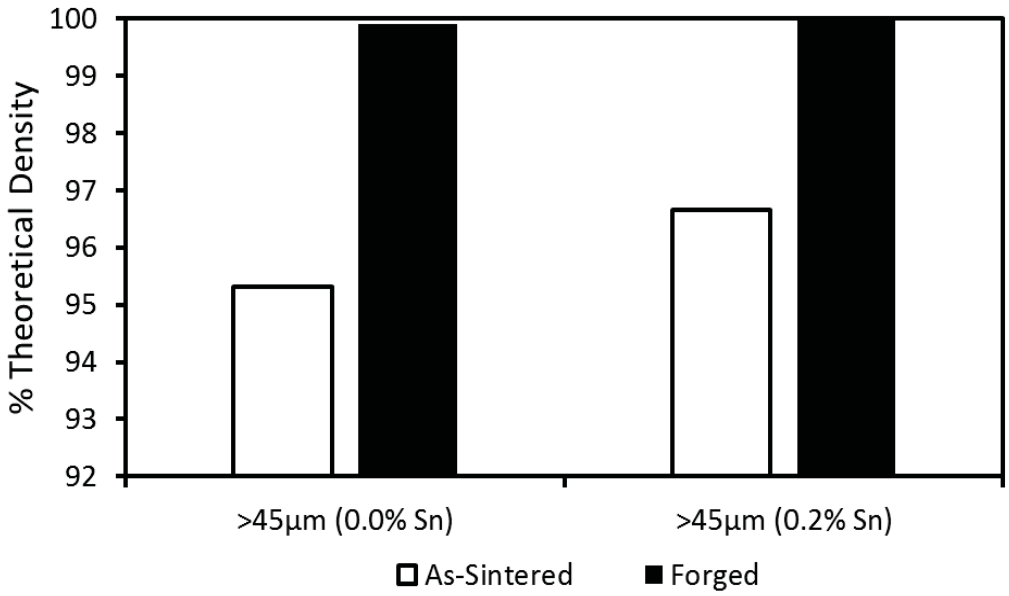

Figure 23: Effects of forging on the density of industrially sintered samples prepared with >45 µm PA7055 powder. All samples pre-heated at 470°C prior to forging.

In an effort to further improve the quality of forged products, additional bars were sintered and then forged using different pre-heat temperatures ranging from 450 to 490°C. All of these products appeared to be crack-free and were effectively fully dense. Hence, they were then heat treated to the T76 condition, machined into tensile specimens, and tested. Plots for the resultant data on yield strength, UTS and elongation to fracture are shown in Figure 24. When looking at the nominal effects of forging temperature, minimal gains were seen when this processing condition was shifted within the range of temperatures considered. However, while additions of tin were shown to be beneficial to densification in sintering, this modifier consistently imparted a detrimental effect on the mechanical properties of the alloy. It was postulated that this was due to the high probability that tin would react to form the brittle intermetallic (Mg_2Sn) [31]. The presence of this phase would have facilitated the noted decline in tensile performance for two reasons. First, was that the negligible solid solubility of tin in aluminum ensured that this phase would reside along the grain boundaries thereby weakening these features and facilitating the propensity for crack propagation. Secondly, its formation would have consumed magnesium, thereby reducing the amount of η ($MgZn_2$)-based precipitates formed within the grain interiors during heat treatment. As such precipitates are essential for maximized yield strength and

UTS, any reduction in their concentration would have a negative impact on the strength of the final product.

Based on these data, the use >45μm PA7055 powder devoid of admixed tin and a forging temperature of 470°C was the most appropriate combination of processing parameters. The latter was selected as it was at the middle of the range considered and coincided directly with the solutionizing temperature of the alloy. Preheating to this temperature thereby allowed forging to be completed in a state where the alloy was soft and comprised of a homogenous microstructure largely premised on a single phase solid solution.

With a seemingly optimal CIP-Sinter-Forge product identified, additional work was then completed to compare this material directly against the wrought counterpart system. Optical images of the etched microstructures for each are shown in Figure 25. It was noted that the powder-derived material maintained a narrow distribution of grain sizes with most being rounded/equi-axed with a nominal diameter of ~70μm. The grain size distribution was more bi-modal in nature within the wrought alloy as select regions exhibited a nominal grain size of ~10-20μm while others were an order of magnitude larger. Additionally, lateral flow was apparent in both materials. However, the general extent of this was much more obvious in the wrought product as evident by highly elongated grains and banding of secondary intermetallic phases.

Both materials were then assessed by means of EBSD to investigate these microstructural differences in greater detail. Maps depicting the crystallographic orientation of grains relative to the longitudinal direction are shown in Figure 26. That for the PA7055 material (Figure 26(a)) revealed that while elongated grains were present, the extent of texture development (and in turn, the anticipated level of anisotropy in mechanical properties) was moderate given that these same grains maintained a diverse range of crystallographic orientations. Conversely, the majority of grains within the wrought counterpart were predominately orientated in a way whereby the [101] direction was parallel to the longitudinal axis thereby indicating the presence of more acute texture development. Data

on the corresponding distributions of grain boundary misorientation angles (Figure 27) revealed additional differences. These results indicated that nearly 80% of the grains in wrought 7055 subscribed to the general definition of a low angle grain boundary (LAGB) wherein the misorientation angle was <15°. As such, the majority of the smaller grains within this material were in fact sub-grains. This fraction was reduced significantly in PA7055 as only 54% were LAGBs.

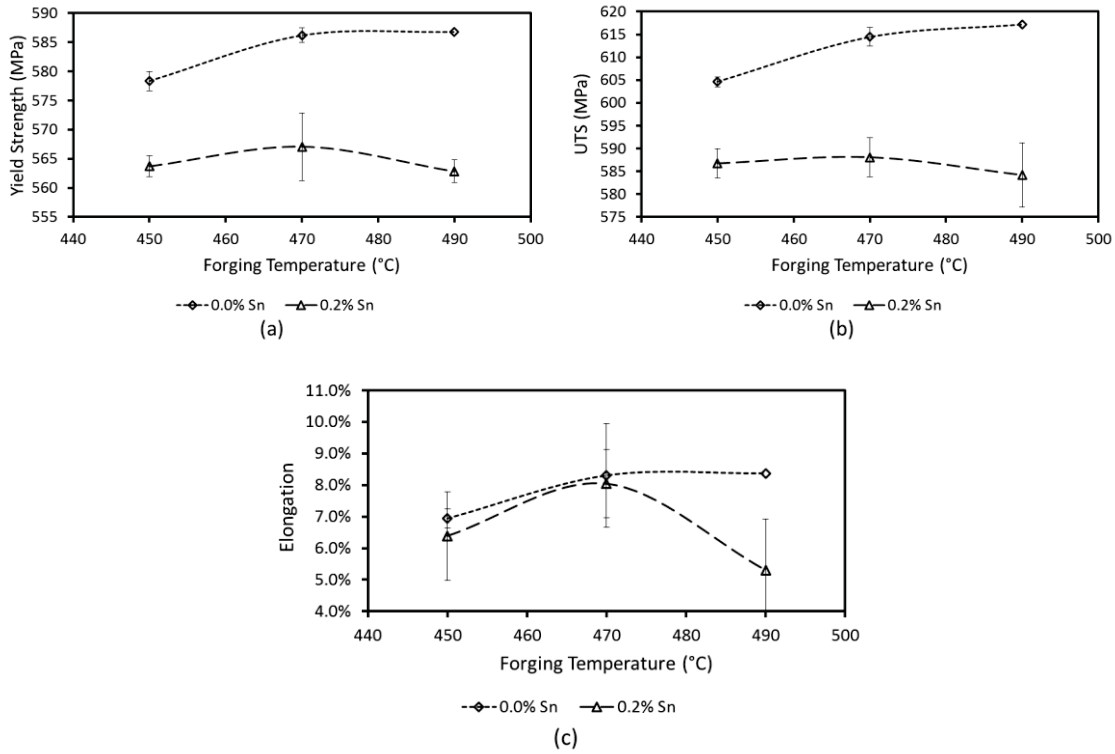

Figure 24: Effect of forging temperature and tin content (wt. %) on the tensile properties of CIP-Sinter-forge specimens consolidated from >45µm PA7055 powder. (a) Yield strength, (b) ultimate tensile strength, and (c) elongation to fracture.

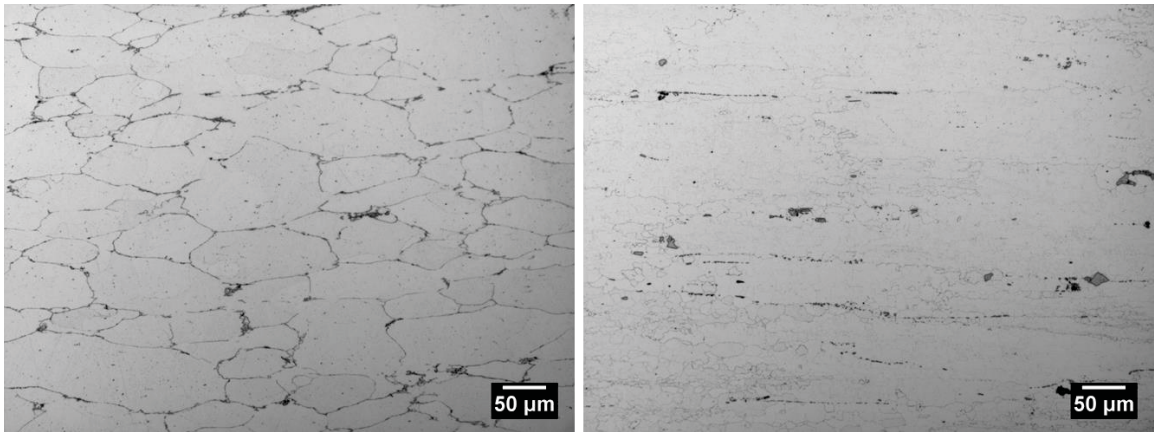

(a) (b)

Figure 25: Comparison of the microstructures observed via optical microscopy in (a) CIP-Sinter-Forged-PA7055-T76 and (b) wrought 7055-T76 after etching with Keller's reagent.

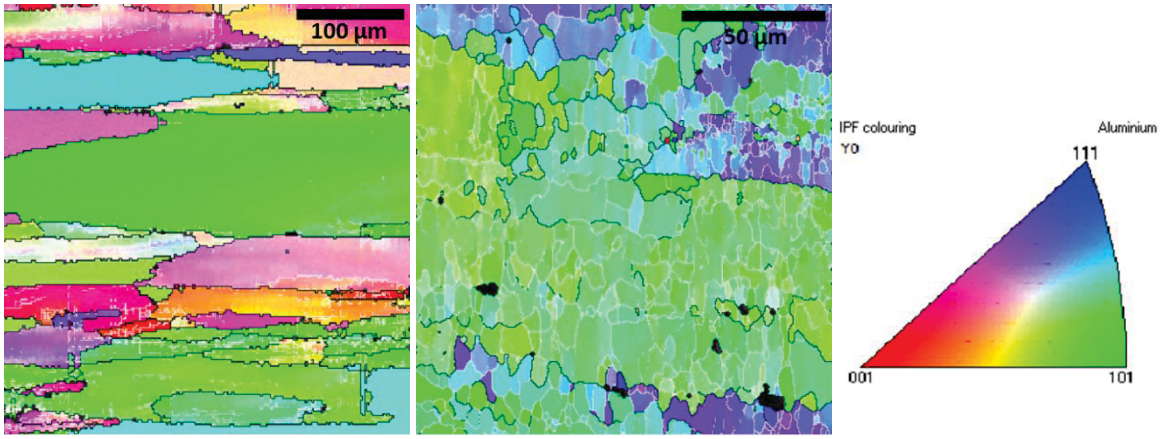

(a) (b) (c)

Figure 26: Maps illustrating the crystallographic orientations of α-aluminum grains found within (a) CIP-Sinter-Forged-PA7055-T76 and (b) wrought 7055-T76 coupled with (c) the corresponding inverse pole figure. White lines indicate LAGBs whereas black lines indicate HAGBs.

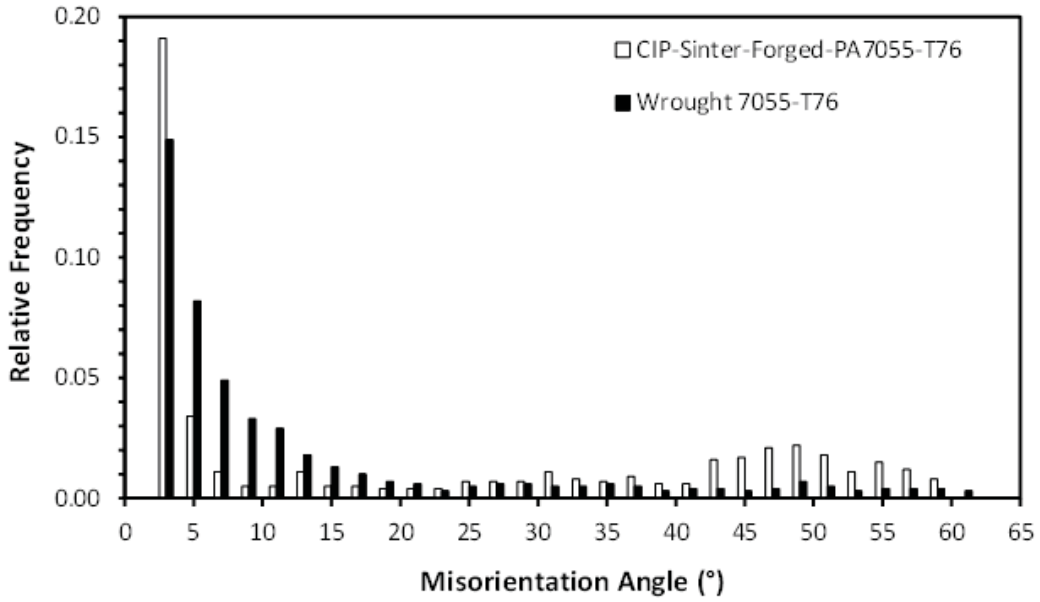

Figure 27: Comparison of the statistical distributions in grain misorientation angles for CIP-Sinter-Forged-PA7055-T76 and wrought 7055-T76.

The final means of direct comparison was that of tensile properties. Average values for the PM and wrought systems are shown in Table 11. Both materials offered an attractive balance of yield strength and tensile ductility. The PM product itself offered modest gains in stiffness and yield strength as the expense of a marginally lower ductility. Such trends were observed in prior studies on PM-derived forged products alloys within the 7xxx [41] and 2xxx [42] series. Here, it was postulated that the transitions stemmed from the existence of a distribution of fine oxide particles within the PM material. These particles were derived from the surface film on the starting raw powders. Hot forging then disrupted the continuity of this oxide network thereby converting these refractory features into a refined strengthening agent within the forged product. Given that the oxygen concentration within the starting PA7055 powder was approximately an order of magnitude higher than that in the wrought counterpart (Table 5), the same logic would be expected to prevail. However, as clear differences in the grain structures of the wrought and PM products were also noted, it is expected that this difference may have also played a contributory role.

Table 11: Comparison of the average tensile properties measured for specimens of CIP-Sinter-Forged-PA7055-T76 and wrought 7055-T76.

Material	**E** (GPa)	**Yield** (MPa)	**UTS** (MPa)	**Elongation** (%)	**Hardness** (HRB)
CIP-Sinter-Forged-PA7055-T76	74 ± 2	586 ± 1	615 ± 2	8.3 ± 1.6	90 ± 1
Wrought 7055-T76	71 ± 1	562 ± 7	611 ± 8	10.4 ± 0.5	90 ± 2

3.5 Conclusions

The overall objective of this research was to investigate the CIP-Sinter-Forge processing response of gas atomized 7055 powder. In meeting this objective the following conclusions were reached:

- PA7055 powder exhibited a moderate response to sintering in a nitrogen atmosphere.
- The general extent of densification was improved with admixed additions of tin while those of magnesium had a detrimental effect.
- The removal of sub-45μm particles from the starting base powder imparted an improved flow rate but was found to reduce the apparent and sintered densities.
- Industrially sintered products demonstrated comparable properties to those sintered in a controlled laboratory setting.
- Hot forging sintered billets of >45μm PA7055 powder at 470°C was found to yield the most desirable PM product within the range of parameters studied.
- CIP-Sinter-Forged PA7055-T76 demonstrated comparable tensile properties and hardness to its wrought counterpart 7055-T76.

3.6 Acknowledgements

The authors would like to graciously acknowledge the financial support provided by Boeing Research and Technology (research contract 11-6392), the Natural Sciences and Engineering Research Council of Canada (NSERC) via collaborative research and development grant #451466 and GKN Sinter Metals. Technical guidance provided by researchers at Boeing (Drs. Steve Gaydos, Ryan Glamm, Marc Froning) is also gratefully acknowledged as is the laboratory assistance provided by colleagues at Dalhousie University (Randy Cooke, Mark Amegadzie, Dean Grijm) and the powder atomization completed by Dr. Bernd Mais (Ecka Granules).

CHAPTER 4. CONSOLIDATION OF AEROSPACE GRADE ALUMINUM 7055 POWDER THROUGH SPS-FORGE PROCESSING

N.P. Kraus and D.P. Bishop
Dalhousie University
Department of Process Engineering and Applied Science
1360 Barrington St., Halifax, Nova Scotia, Canada, B3J 1Z1

R.L. Hexemer Jr. and I.W. Donaldson
GKN Sinter Metals LLC
2200 N. Opdyke Road, Auburn Hills, USA, 48326

Status: Submitted, Canadian Metallurgy Quarterly, August 2016

The following experimental procedures, results and discussions were completed by N.P. Kraus, with reviewer and editorial roles played by the co-authors.

Abstract

The objective of this research was to assess the SPS-forge response of fully pre-alloyed aerospace grade 7055 (Al-8Zn-2.1Mg-2.3Cu-0.2Zr) powder. The core variables investigated were the sintering temperature, time, and atmosphere employed, as well as the average particle size and the manner of uni-axial loading. Samples sintered in vacuum at 500°C for 40 minutes with delayed loading offered the most desirable combination of density, hardness, and bend properties but remained relatively brittle. Hot forging the sintered preforms was found to impart sizable gains in mechanical properties. The SPS-forge product exhibited tensile yield strength of 603MPa coupled with a ductility of 9.1% and a hardness of 93 HRB. All such properties were largely equivalent to those measured for the wrought counterpart.

4.1 Introduction

Spark Plasma Sintering (SPS) is a material processing technique that is characterized by a simultaneous application of current and pressure to a powder bed in an effort to attain a high density product. Here, a current which is often applied in a pulsed DC wave pattern (normally on the order of 10's of volts and thousands of amps), is utilized to directly heat the powdered material. In the situation where the current is able to pass through the powder bed, as is the case for electrically conductive powders, heating occurs through the principles

of Joule heating [55]. Additional heating occurs due to the flow of current through the die set utilized as this must be made from an electrical conductor; typically, high purity, high density graphite [52].

When producing samples through SPS numerous parameters have been shown to have a large impact on the final product. Some of the most influential include, pressure, temperature, and the time when the pressure is applied. Other studies have also looked at the effect on heating rates [52], and DC pulse pattern [53]. Overall many different alloy systems and process parameters have been investigated. One of the most extensive overviews of SPS work was conducted by Orrù et al. and published in 2009. This work references some 1000 papers conducted on approximately 80 different metallic and ceramic systems [54]. In Orrù's paper, the materials successfully consolidated via SPS range from pure metals such as aluminum, iron, nickel and titanium to the SPS of carbides, borides nitrides and oxides including Fe_3C, WC, AlN, TiN, TiO_2, MgO and Al_2O_3.

In the case of metallic aluminum several SPS studies have focused on transitions in the oxide films present on the powder particles along with the effects of retained impurities within sintered compacts [66][67][68][69][73]. While the majority of this work has been focused on aluminum powders with relatively simple chemistries, considerable work has also been completed on more complex aluminum alloys including members of the 2xxx [74][51], 5xxx[75] and 7xxx[77][78][85] series. In general it has been found that higher sintering temperatures allow for enhanced breakdown of the oxide shell which increases the frequency of metal/metal bonding between particles [68]. It has also been found that the temperature at which pressure is applied can have a great impact on the final properties of the material [68][71][86].

Overall, some very promising results have been realized when studying the SPS of aluminum alloys. This includes finished products with wrought-like mechanical properties [73][71] as well as nano-scale microstructures [76]. Other works have shown that by controlling the post-SPS cooling rate, samples were able to maintain a state of

supersaturation comparable to the starting powder which was produced through rapid solidification [85]. This scenario enabled direct aging of the SPS product so as to avoid the need for a complete solution-heat treat process.

Although the list of aluminum powders investigated through SPS is certainly growing, numerous alloy formulations of commercial importance have yet to be considered. Many of these unstudied alloys are based on modern wrought systems utilized in aerospace applications. A key example of which is the high zinc alloy 7055. This particular alloy offers exceptional compressive strength and has now replaced conventional members of the 7xxx series such as 7075 and 7150 in an array of aerospace structures. Hence, the objective of this work was to conduct a fundamental study on the SPS response of 7055 powder.

4.2 Materials

The aluminum alloy of interest in this study was grade 7055 (Al-8Zn-2Mg-2.3Cu-0.2Zr). Initially sourced as wrought plate, this raw material was then gas atomized into fully prealloyed powder at Ecka Granules (Furth, Germany) and subsequently sieved to remove the majority of powder particles <45μm. Hereafter, the powder is denoted as "PA7055". A particle size distribution for the screened PA7055 was attained through laser light scattering as shown in Figure 28. The powder was found to have a rounded/spherical morphology and a cellular microstructure (Figure 29). Chemistries of the wrought and powdered materials were verified through inductively coupled plasma optical emission spectrometry (ICP-OES). As seen in Table 12 the chemistries of both materials were well aligned with the accepted chemical tolerances for 7055 as specified by the Aluminum Association.

Table 12: Assays of the materials utilized. All values in weight %.

Material	Chemistry	Al	Zn	Mg	Cu	Zr
7055	*Specification*	*Bal*	*7.6 – 8.4*	*1.8 – 2.3*	*2.0 – 2.6*	*0.1-.025*
Wrought 7055	Measured	Bal	7.97	1.85	2.12	0.16
PA7055	Measured	Bal	8.06	2.10	2.39	0.11

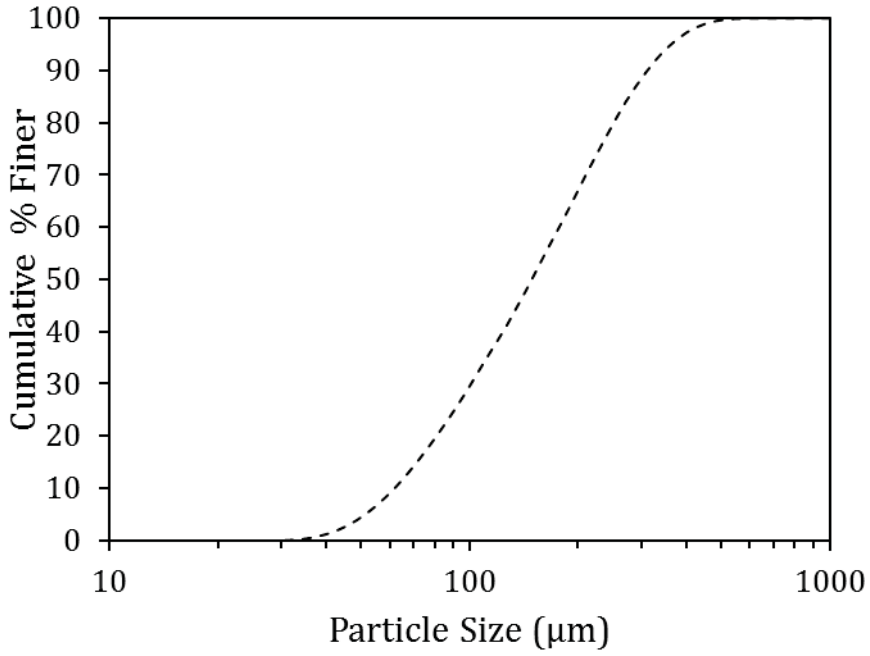

Figure 28: Particle size distribution for the PA7055 powder.

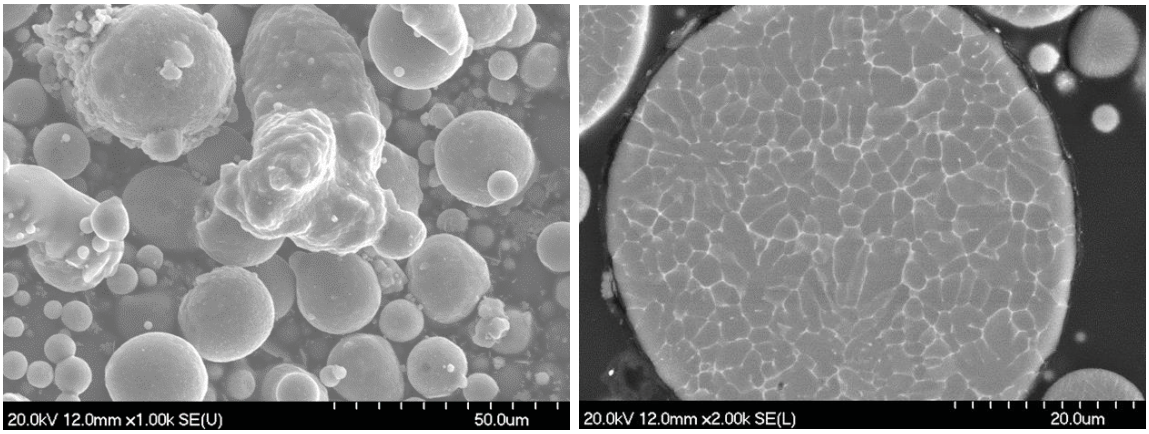

(a) (b)

Figure 29: Images illustrating the typical (a) morphology and (b) internal microstructure of PA7055 powder.

4.3 Experimental Techniques

All samples utilized in this study were processed in a Model 10-3 SPS manufactured by GT Advanced Technologies equipped with graphite tooling designed to produce cylindrical samples (40mm diameter x ~15mm thick). This particular model had a maximum current of 3000A at 10V. Sintering temperatures ranged from 150 to 500°C while sintering times of 120s, 600s and 2400s were considered. The majority of specimens were consolidated under a mechanical vacuum atmosphere ($2x10^{-2}$ Torr) although static atmospheres of high purity nitrogen, argon, and helium were considered in select instances. Standardized parameters included a heating rate of 50 K/min and current applied as a pulsed-DC wave form with a 25ms on, 5ms off pattern. A peak pressure of 50MPa was also common to all samples although the manner of application differed. Here, two different modes of pressure application were utilized (Figure 30). Under Type I conditions, peak pressure was applied at the start of the run and then temperature was ramped as needed. In Type II conditions as denoted by Zadra et al. [71] and Liu et al. [86], the peak pressure was not applied until the sample reached the intended sintering temperature. Degassing response was assessed using a Netzch thermogravimetric analyzer (TGA) coupled with a gas chromatography-mass spectrometry (GC-MS) system. Here, powder samples (1 g) were heated at 50°C/min to a peak temperature of 500°C under an atmosphere of helium with a reported purity of 99.999%. With this apparatus researchers were able to analyze the gases emitted from the loose powder as a function of temperature. SPS products were then machined into cylinders

(12mm diameter x 38mm length), preheated to 470°C, and hot rotary forged to achieve a net reduction in cross sectional area of ≈50%. Prior to mechanical testing, all specimens (SPS and SPS+Forge) were heat treated to the T76 condition. This involved solutionizing at 472 ± 5°C for 5400s, followed by water quenching, and two-step aging (18ks at 121°C followed by 25ks at 160°C).

Characterization of consolidated products involved a number of techniques. Density was measured using standard Archimedes principles combined with oil infiltration and water immersion. Measured values were then divided by the full theoretical density of the alloy (2.861 g/cc) and converted into a percentile value. Samples for microscopy studies were mounted in epoxy and then polished using a conventional series of grinding and polishing steps. SEM analysis was then performed using a Hitachi S-4700 microscope operated with an accelerating voltage of 20kV and a beam current of 15mA. Mechanical property measurements included hardness, three point bend strength, and tensile properties. Hardness was measured in the HRB scale using a Wilson Rockwell 2002 machine. Three point bend tests were executed following the protocols detailed in ASTM B528 and B925. Rectangular bars (31.7 x 12.7 x 6.0 mm) machined from SPS pucks were utilized for this purpose. Each bar was loaded in an Instron Model 5594-200HVL frame equipped with a 50kN load cell until fracture. The ultimate bend strength (UBS) was then calculated based on the peak load and cross sectional area of the test bar. For tensile tests, forged rods were machined into threaded end bars in accordance with ASTM E8-M and tested using the same frame employed for three point bend measurements. Engineering strain was recorded with an Epsilon model 3542 extensometer that remained attached through the point of fracture.

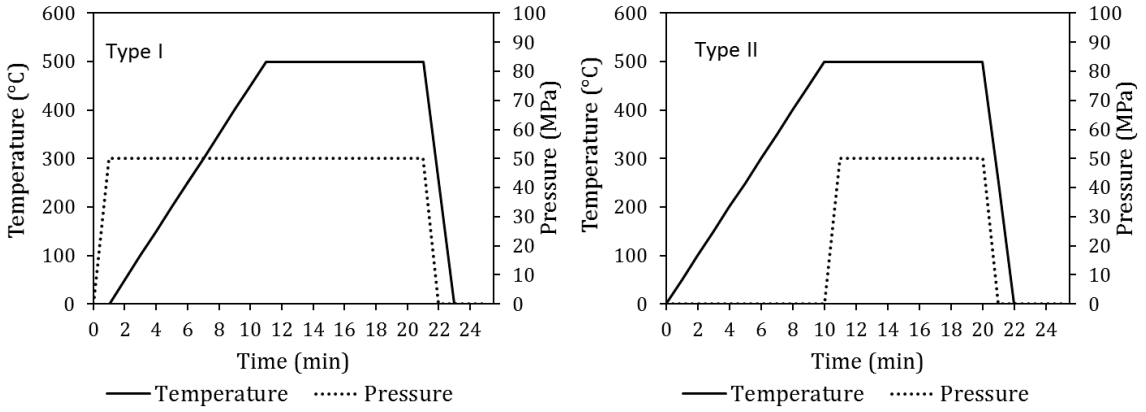

(a) (b)

Figure 30: Transitions in the SPS temperature and pressure followed during (a) Type I and (b) Type II processing.

4.4 Results and Discussion

4.4.1 Effect of SPS Parameters

The initial segment of research emphasized studies on the SPS variables that are typically the most influential; namely, sintering temperature and sintering time. In both instances, counterpart specimens were produced using Type I and Type II loading modes.

4.4.1.1 Effect of Sintering Temperature

Resultant data on density as a function of sintering temperature are presented in Figure 31. Points derived from Type I processed pucks revealed that a steep transition in densification occurred as sintering temperature increased from 200°C to 400°C. At the lower end, densification was minimal as the final densities remained well below the full theoretical maximum. However, near full densification was achieved at sintering temperatures ≥400°C. Here, an effective plateau in the data was observed although the highest value was measured from pucks processed at 500°C (99.8%). The plateau trend and measured densities were effectively identical in a counterpart series of pucks fabricated in accordance with Type II processing. These findings indicated that 500°C was a promising temperature for SPS processing of PA7055 powder and that the loading mode had no obvious impact on densification. SPS temperatures in excess of 500C°C were of interest but could not be

considered given the potential for evaporative loss of zinc and the subsequent contamination of the SPS apparatus that would transpire if this were to occur.

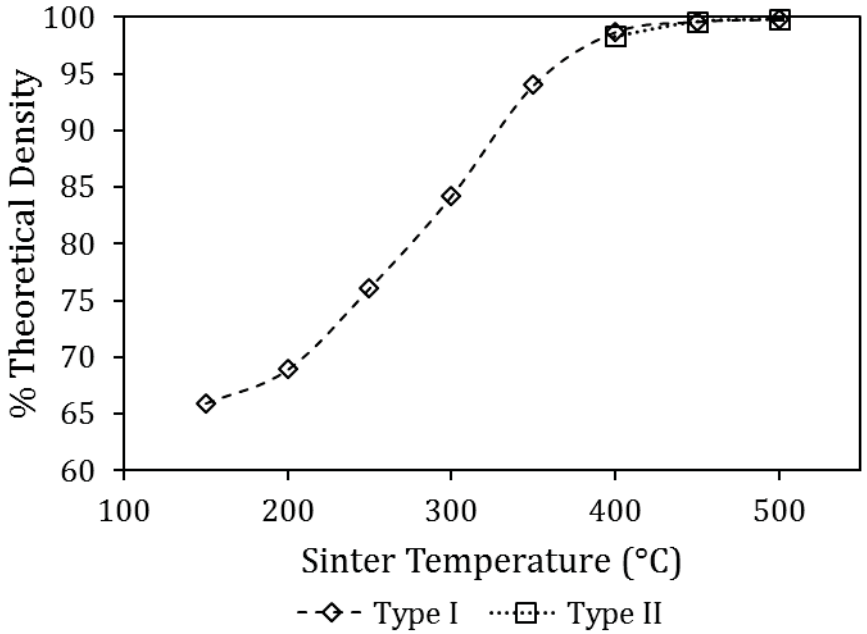

Figure 31: Effect of SPS temperature on the densification of PA7055 powder. All specimens held at temperature for 120s.

It was determined that densification trends in Type I and Type II samples both correlated well with obvious transitions in sinter quality and the extent of residual porosity. Micrographs illustrative of this are provided in Figure 32. With a sintering temperature of 300°C, residual porosity was clearly abundant. It also appeared that inter-particle necking had commenced but the size of these bonds was limited. As the sintering temperature was further increased to 350 and on to 400°C there was a continued reduction in porosity and an increase in inter-particle bonding. At a sintering temperature of 450 and 500°C minimal evidence of residual porosity and prior particle boundaries was observed. At both of these temperatures the sample was ~100% dense as noted in Figure 31.

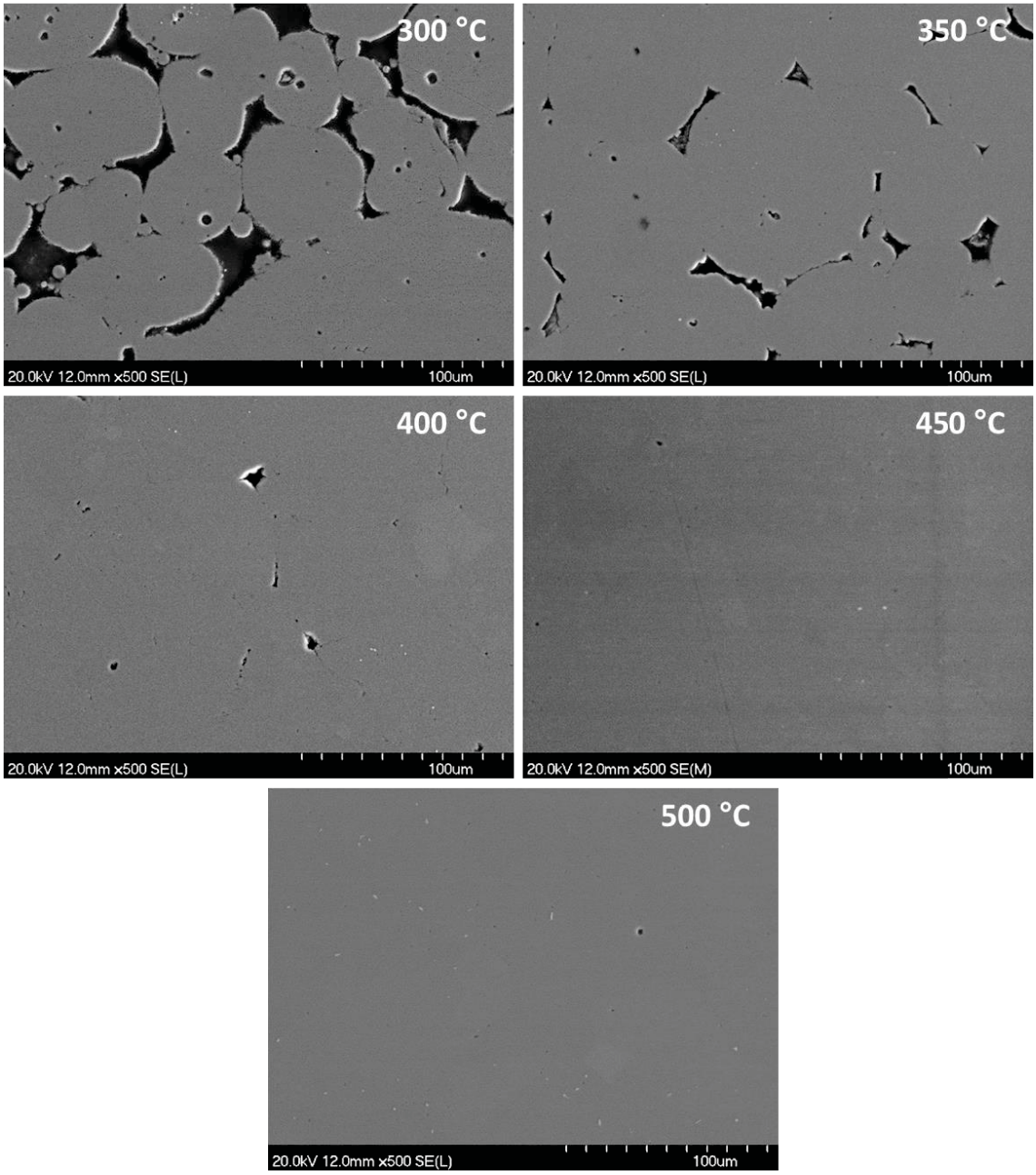

Figure 32: Evolution of the microstructure within PA7055-T76 specimens with progressive increases in SPS temperature. All specimens held at temperature for 120s (Type I). Porosity is black.

Mechanical property data were then acquired through hardness measurements and three point bend tests on specimens heat treated to the T76 state. Data on the former are shown in Figure 33. Such tests were limited to pucks SPS processed at temperatures ≥300°C as those consolidated at lower temperatures were excessively brittle and fractured

immediately upon contact with the indenter. Akin to the trend observed in sintered density, hardness also increased sharply from 300 to 400°C but then plateaued at higher SPS temperatures. Similarly, 500°C sintering yielded products with the greatest hardness while loading mode had no obvious impact. For instance, the average hardness of Type I and Type II samples sintered at 500°C were 92.3 ± 0.7 and 92.8 ± 1.1 HRB respectively.

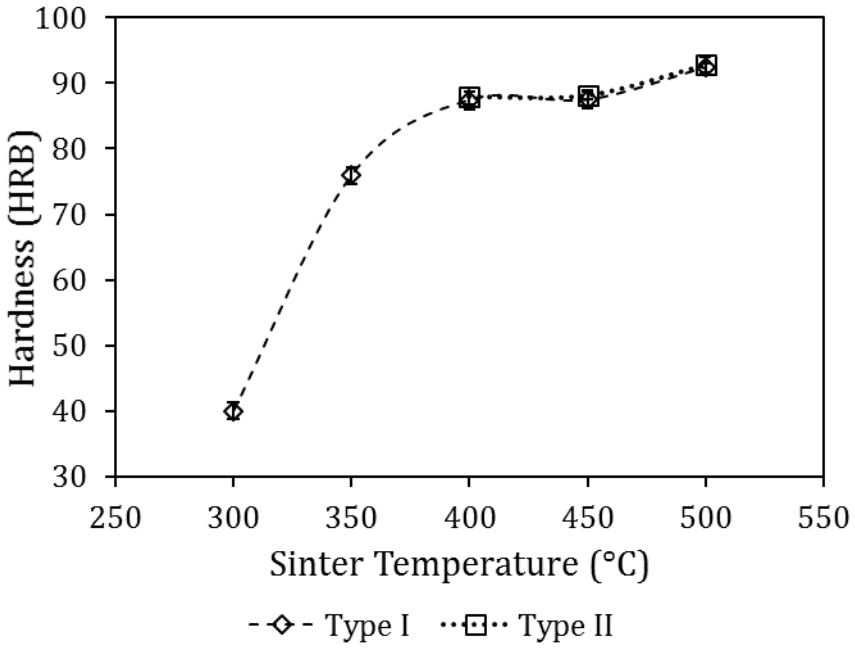

Figure 33: Effect of SPS temperature on the hardness of PA7055 specimens following T76 heat treatment. All specimens held at temperature for 120s.

Three point bend tests were limited to samples consolidated at a minimum of 400°C given that lower temperatures yielded products with unacceptably low density, hardness, and sinter quality. UBS data (Figure 34) indicated that this attribute was dependant on sintering temperature as well as the mode of loading. For example, with Type I processing, UBS doubled from ~75MPa to ~150MPa with rising SPS temperature. While this upward progression was desirable, the values remained inferior to those measured for other aluminum-based powders consolidated by SPS wherein strengths >300MPa have been measured [87][77]. They were also greatly inferior to the UBS of wrought 7055-T76 for which a value of 1485MPa was measured. Alternatively, with Type II processing the UBS

strength tripled with increasing sinter temperature from ~140 to ~430MPa. Furthermore it was noted that across all sintering temperatures there was a large gain when using the Type II mode of pressure application.

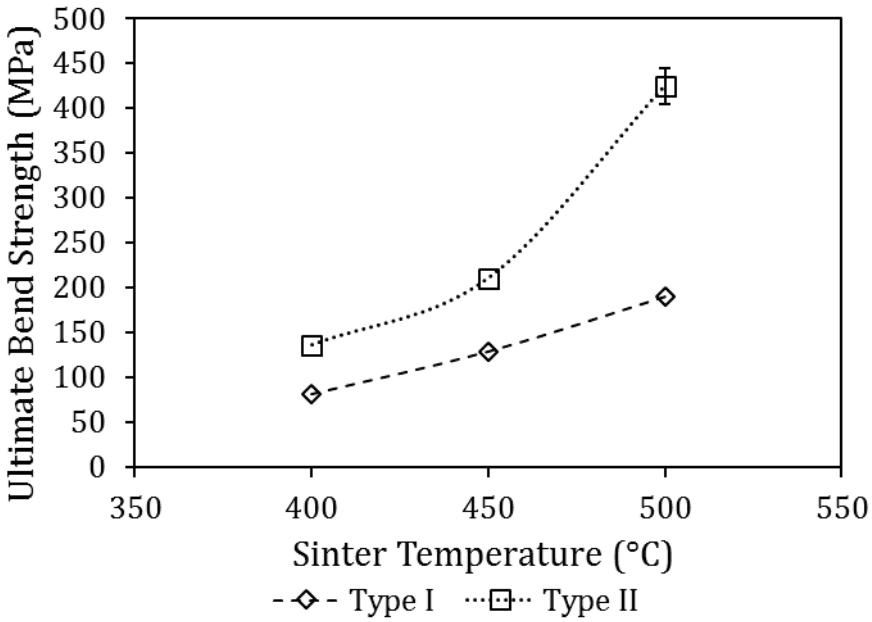

Figure 34: Effect of SPS temperature and loading mode on the UBS of PA7055-T76 specimens. All products held at temperature for 120s.

4.4.1.2 Effect of Sintering Time

To further assess the effect of changing SPS parameters, the influence of hold time at sintering temperature was investigated. In these trials all other parameters were held constant and a sintering temperature of 500°C was utilized. The sintering time presented represents the amount of time that the samples were held at peak temperature while under the application of the applied pressure (50MPa). When looking at the data collected (Table 13) no obvious trend could be seen with respect to hardness or density with increasing sintering time or change in pressure application mode.

Table 13. Effect of sintering time at 500°C on the hardness and density of PA7055-T76 specimens consolidated under Type I and Type II modes of processing.

Loading Mode	Sintering Time (Sec)	Hardness (HRB)	Sintered Density (% Theoretical)
Type I	120	92.3 ± 0.7	99.8
	600	92.3 ± 0.8	99.9
	2400	92.7 ± 0.8	99.9
Type II	120	92.8 ± 1.1	99.9
	600	93.2 ± 0.3	99.5
	2400	92.0 ± 1.2	99.8

Data showing the effect of sintering time on UBS are presented in Figure 35. Type I processed specimens maintained a low UBS of ~150-200MPa over the full range of sintering times considered. This nominally static response was consistent with the measured transitions in density and hardness (Table 13) as neither of these properties were influenced by sintering time either. Interestingly, data from Type II processed materials were in stark contrast. Here, a progressive improvement in UBS was noted as sintering time was extended with a peak value of 734MPa measured. Accordingly, the sizable advantage instilled through Type II processing under a hold times of 120s and 2400s was amplified from 125% to 260% respectively. A similar response was also noted in works by Zadra [71] and Liu et al. [86] whom stated that the change in mode of pressure application had a large effect on mechanical properties while density and hardness were largely unaffected.

Of the three properties measured, UBS was unique in that it involved the development of tensile stress within the specimen thereby presenting it as the only metric of inter-particle bond quality. Establishing high-quality metallurgical bonds between the starting powder particles is by no means trivial given the complex oxide/hydroxide chemistry that exists at the surface of the powder particles. This layer typically impedes sintering because it is thermodynamically stable during sintering. For instance, the reduction of Al_2O_3 at 600°C would mandate a partial pressure of oxygen $<10^{-50}$ atm [34]. As this P_{O2} is not attainable,

the oxide layer is stable throughout conventional sintering and thus impedes the formation of strong metal-metal bonding between adjacent powder particles. This problem is further exasperated by the fact that the oxide layer has a strong tendency for hydration [88]. As such the aluminum powder is covered with an oxide layer containing physisorbed (H_2O) and chemisorbed ($Al_2O_3 \cdot 3H_2O$) water. Such contaminants are then incorporated into the final product. This has been shown to lead to inferior ductility as well as cracking and blisters within products and as such the degassing nature in aluminum has been widely studied [50][89][90][91][92]. These studies show that as temperature is increased, physisorbed water is first evaporated off at temperatures up to ≈175°C [50] [90], followed by the decomposition of chemisorbed water. This decomposition of the chemisorbed water has been shown to happen over a wide range in temperatures up to ≈550°C [50] [91] [92] . At higher temperatures ≈200 – 450°C the release of hydrogen has been shown to be dominant and is caused by metallic aluminum and/or magnesium reacting with water vapor liberated at lower temperatures [90].

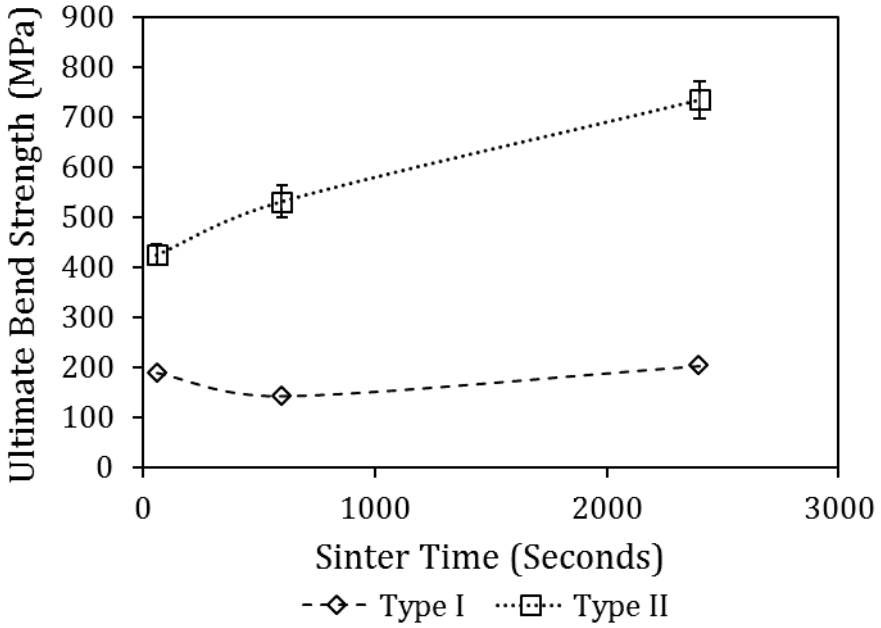

Figure 35: Effect of sintering time on the UBS of PA7055-T76 specimens consolidated at 500°C.

In an effort to understand the mechanism(s) responsible for the differences between Type I and Type II styles of processing, powder off-gassing coupled with information on ram displacement within the SPS system were considered. The former was studied by heating a sample of the loose powder within a TGA/GC-MS. The resultant data (Figure 36) indicated that there was an obvious release of gaseous water and carbon dioxide upon heating. Water was released at temperatures ranging from 100 to 380°C with the bulk of off-gassing transpiring from 170 to 280°C. Conversely, the range coinciding with carbon dioxide release was somewhat broader (100 to 450°C) and occurred as a sharper peak at 325°C. When conducting SPS at 500°C, both degassing events should have occurred to the full extent noted. However, it was hypothesized that Type II processing would allow for a more effective release of the liberated gasses as the compact maintained a relatively low density while it was heated through the temperatures when degassing events were most active.

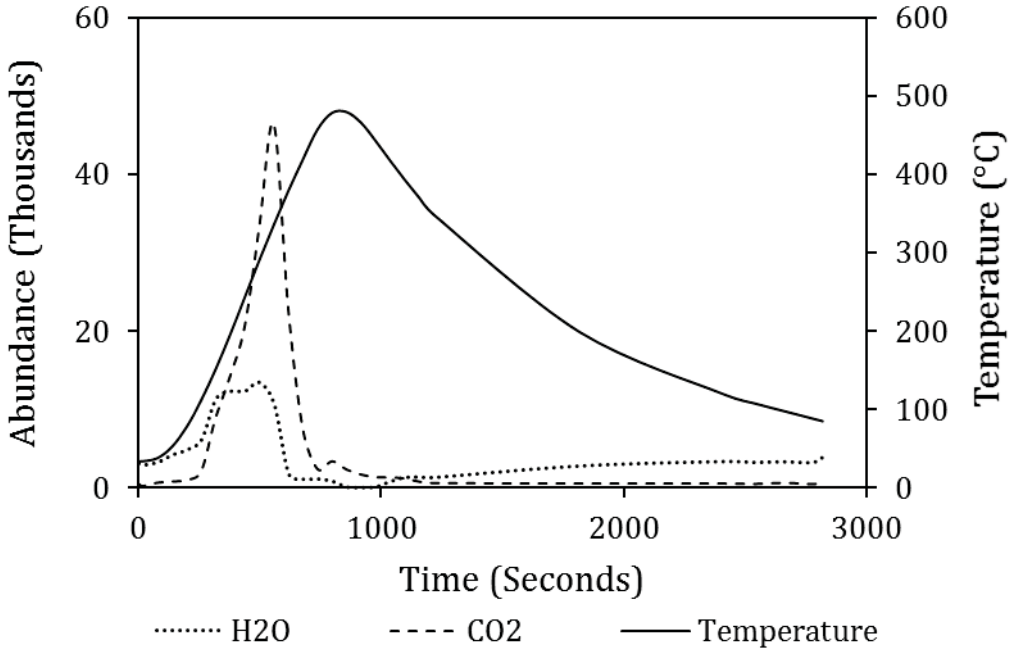

Figure 36: Off-gassing of H_2O and CO_2 from PA7055 powder as a function of temperature.

Evidence that a lower density prevailed was deduced through an assessment of the ram displacement data shown in Figure 37. Inspection of theses profiles for Type I and Type II

processing sequences indicated that clear differences had transpired as five key stages (denoted (1) to (5)) were observed for the former yet only four (denoted (A) to (D)) were noted for the later. In Type I (Figure 37 (a)) the initial application of pressure brought about an immediate and steep incline in ram displacement (stage (1)) indicative of a gain in density. As this loading was executed at room temperature, it was clear that rearrangement of the powder particles within the die was responsible for this transition. The extent of ram displacement was then reduced slightly during the early stages of heating up to ~150°C (stage (2)). At this point the ram position was governed by the natural thermal expansion of the powder as the level of heat input was inadequate for sintering-induced densification. Ram displacement then increased markedly from 150°C to ~420°C (stage (3)) after which point it remained effectively static to the end of the sintering hold period at 500°C (stage (4)). Hence, it was evident that the bulk of densification derived from current flow and pressure had occurred within the third stage of the cycle. Release of the pressure at the end of the hold time allowed the consolidated product to spring back and thereby sharply decrease ram displacement. This was followed by a gradual increase in displacement (now under a low load of only 5MPa) as the compact shrank due to natural thermal contraction (stage (5)).

The ram displacement profile for a Type II processed material (Figure 37 (b)) was notably different. In this mode of processing, ram displacement began at zero and shifted into negative values once heating commenced and powder underwent thermal expansion (stage (A)). This continued to a temperature of ~220°C at which point the downward trend was reversed and ram displacement began to rise thereby indicating an improving density within the specimen (stage (B)). The displacement change was somewhat gradual up to the peak temperature (500°C). This was then followed by a sharp spike (from ~3 mm to 5.2 mm ram displacement) with the abrupt pressurization to 50MPa (stage (C)). The cycle then concluded with a sharp spring back upon the release of pressure followed by gradual increase in displacement due to thermal expansion (stage (D)).

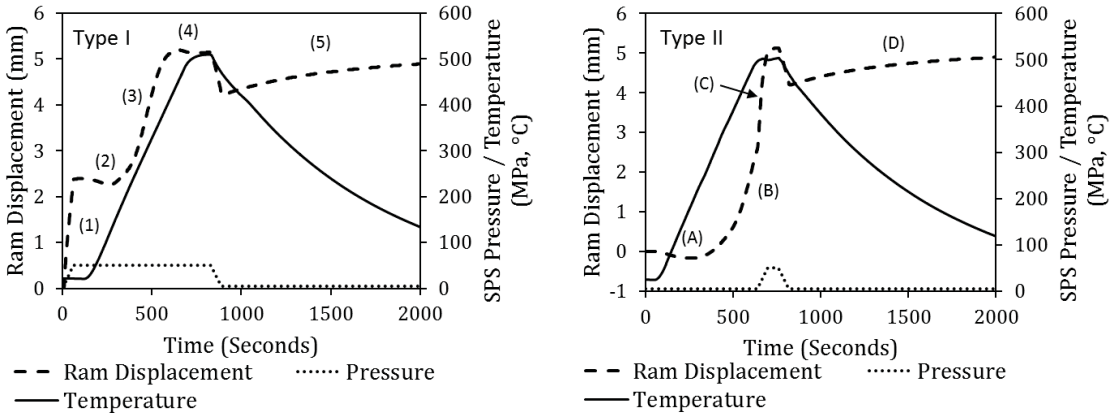

(a) (b)

Figure 37: Figure 10: SPS ram displacement profiles measured during (a) Type I and (b) Type II processing sequences. Samples sintered at 500°C with a 120s hold time.

Collectively, it was postulated that the aforementioned differences in ram displacement profiles were responsible for the distinctly different trends in UBS for Type I and Type II processing as they influenced the general extent of (i) degasssing and (ii) oxide shell rupture. For degassing, it is invariably desirable to maximize this event prior to densification as entrapped gases can have a decisively negative impact on mechanical properties. In Type I processing, densification started early in the cycle with the most acute increase occurring thermally-concurrent with the principal degassing events (Figure 36). This had likely promoted gas entrapment within the material to the detriment of UBS. Conversely, in a Type II sequence, densification was delayed until higher temperatures were reached. This would have left the sample in a relatively porous condition when the release of H_2O and CO_2 were most active so as to intensify degassing and facilitate higher UBS values. The impact of improved degassing would have been most intense within samples sintered for a short period of time as the effect would be exhausted once significant densification had occurred. Hence, it was likely the principal contributor in the UBS differences noted between samples sintered for 120s.

Regarding oxide shell rupture, a critical difference was that the abrupt application of uni-axial pressure occurred at room temperature in a Type I process but was delayed to 500°C in the Type II sequence. It was postulated that the associated deformation within the latter

would have ruptured the oxide shell to a greater extent given the relatively soft nature of the powder and in doing so, facilitated a greater level of metal-to-metal inter-particle contacts. Once established, inter-particle diffusion would have then transpired to a progressively greater extent as sintering time was extended, fostering more intensive bonding and a progressive increase in the UBS (Figure 35). This hypothesis is further supported by the work of Xie et al. which showed that increasing the loading pressure at a higher temperature, promoted a more effective breakdown of the oxide shell [66][67][68][69].

4.4.2 Effect of SPS Atmosphere

When sintering any powdered aluminum, the sintering atmosphere (and selection thereof) invariably plays a critical role. For instance, sintering atmosphere can help to aid in the removal of volatile products that stem from the powder itself and/or admixed process control agents while exerting an impact on critical chemical reactions such as controlled nitridation and oxidation [30]. Indeed, many studies have addressed the role of atmosphere within the confines of conventional, pressureless sintering of aluminum. Here, a superior sinter quality transpires with a nitrogen atmosphere while other options such as vacuum, dissociated ammonia, argon and hydrogen are less effective [93][94][33][30]. Such studies implied that sintering atmosphere could also be influential in SPS as well. Hence, a series of samples were SPS processed at 500°C for 120s under Type II loading in different static atmospheres and tested in three point bending. Data on the UBS are shown in Figure 38. These results indicated that mechanical vacuum was much more effective than any of the gaseous options considered. This was likely due to the fact that under a vacuum atmosphere, the degassing of PA7055 powder (Figure 36) was simply more effective given the low pressure and the fact that the degassed species would have been continually pulled away from the compact. Use of a static gas atmosphere would have been less effective thereby ensuring that the contacting powder surfaces would have still contained physisorbed and/or chemisorbed species that inhibited sintering.

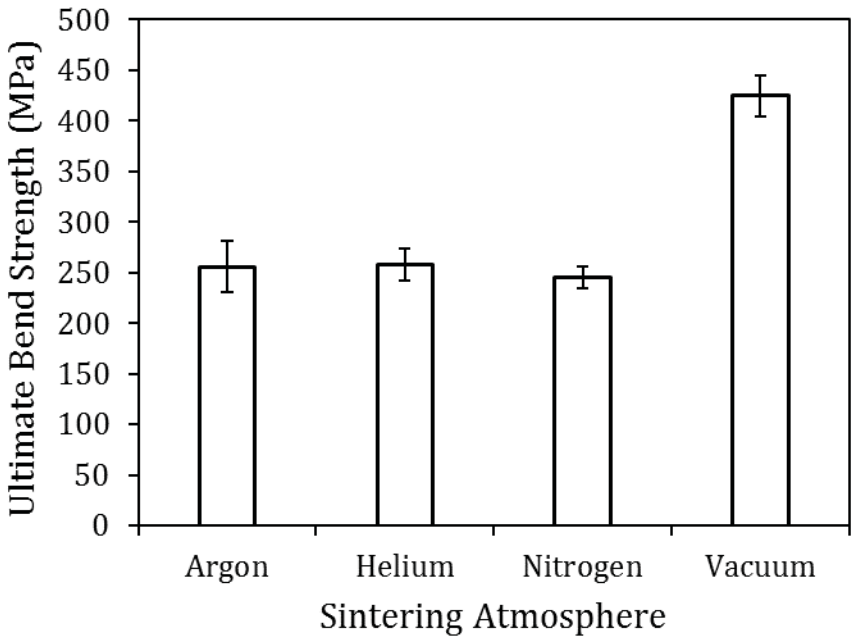

Figure 38: Effect of sintering atmosphere on the ultimate bend strength of PA7055 specimens consolidated at 500°C (Type II; 120s hold time).

4.4.3 Effect of Particle Size

Similar to the investigation on sintering atmosphere, additional samples were produced using selective cuts of powder with an aim to further increase the mechanical performance of SPS products. Here pucks were produced from 6 different cuts. All samples were consolidated using a Type II sequence under vacuum with a sintering temperature and time of 500°C and 120s respectively. Specimens produced with powders screened to a size x<45µm were found to be extremely brittle and did not survive machining. This behaviour was attributed to weak inter-particle bonding exasperated by the increased amount of powder surface area present. Aside from this one problematic cut, all others were readily processed into a coherent product and no meaningful differences in density or hardness were observed. In all cases the samples had a hardness of ~92HRB and were 100% dense. Data on the UBS of these specimens are shown in Figure 39. When comparing these findings to the counterpart sample with only fines removed (425MPa UBS), a slightly higher UBS could be attained by using powders in the range of 75 to 150µm (460MPa). However, this was not perceived to be a gain of any practical relevance given that nearly 80% of the starting powder product would be wasted when pursing this small improvement.

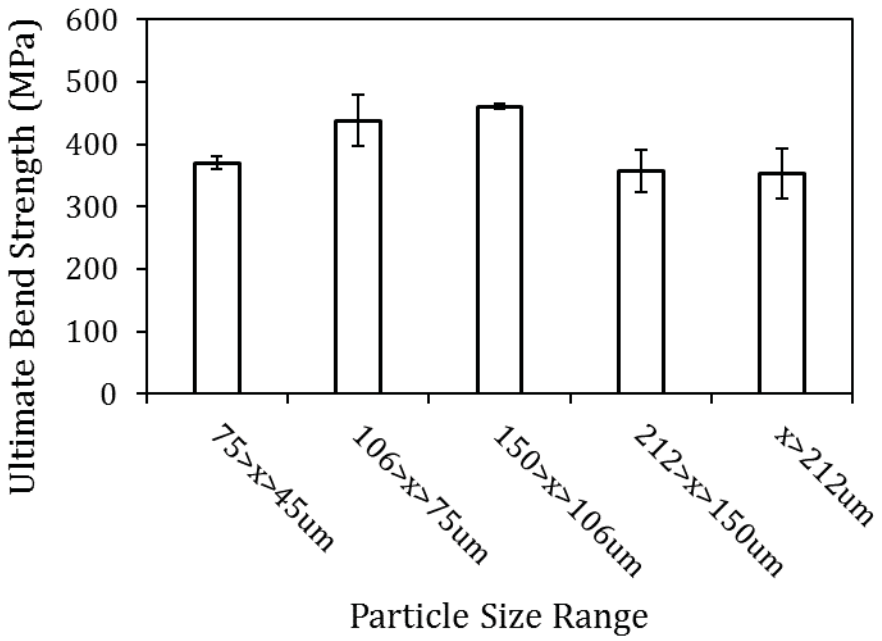

Figure 39: Effect of average particle size on the ultimate bend strength of PA7055 specimens consolidated at 500°C (Type II; 120s hold time).

4.4.4 Effects of Forging on SPS Product

Based on the collective body of data realized, the most desirable samples were fabricated by SPS with a Type II mode of pressure application at 500°C for 40 minutes in a vacuum atmosphere. Although such parameters yielded a product with the highest UBS, this "optimally produced" sample still demonstrated low levels of ductility and relatively low UBS strength as compared to the measured value for wrought 7055-T76 (1485MPa). Hence, to further increase the mechanical properties of such samples a forging step was applied. The etched microstructure of both the SPS-Forged and wrought 7055 samples (rolling direction left to right) are compared in Figure 40. From these microstructures it was noted that the SPS-Forged product maintained its rounded/ equi-axed grain structure with some level of lateral flow apparent. While in contrast, the wrought material showed a much larger texturing effect caused by rolling to a point that there was banding of the secondary intermetallic phases. These findings were very similar to that presented for an optimally produced CIP-Sinter-Forged 7055 product presented by Kraus et al. [95]. Furthermore the SPS-Forged product maintained a narrower particle size range while the wrought material seems to have areas of small sub-grains and areas of exceptionally large grains.

Unlike SPS processed pucks, forged products were of a geometry sufficient for the machining of miniature tensile bars. From Table 14 it can be seen that the tensile properties of samples after hot forging were within 6% of the values measured from identical specimens machined from wrought 7055-T76 plate. This substantial increase in the mechanical properties of post forged products can be explained by looking at other forging trials conducted on PM aluminum alloys from the 2xxx [42] and 7xxx series [41][95]. In these studies it was postulated that gains in the mechanical properties were attributed to the presence of a finely distributed oxides within the sintered PM product formed by disrupting the remnants of the oxide network present within the sintered product during forging. These finely distributed oxide particles ultimately served as a refined strengthening agent within the forged products. It was postulated that the same strengthening mechanism prevailed in the SPS-forge product as well.

Table 14: Comparison of the tensile properties measured for wrought and SPS-Forge variants of 7055-T76.

Process	Young's Modulus (GPa)	Yield (MPa)	UTS (MPa)	Ductility (%)	Hardness (HRB)
SPS-Forged	70.0 ± 2.2	603 ± 1	629 ± 2	9.1 ± 1.2	93 ± 0
Wrought	70.7 ± 1.5	628 ± 6	668 ± 3	13.5 ± 0.4	90 ± 2

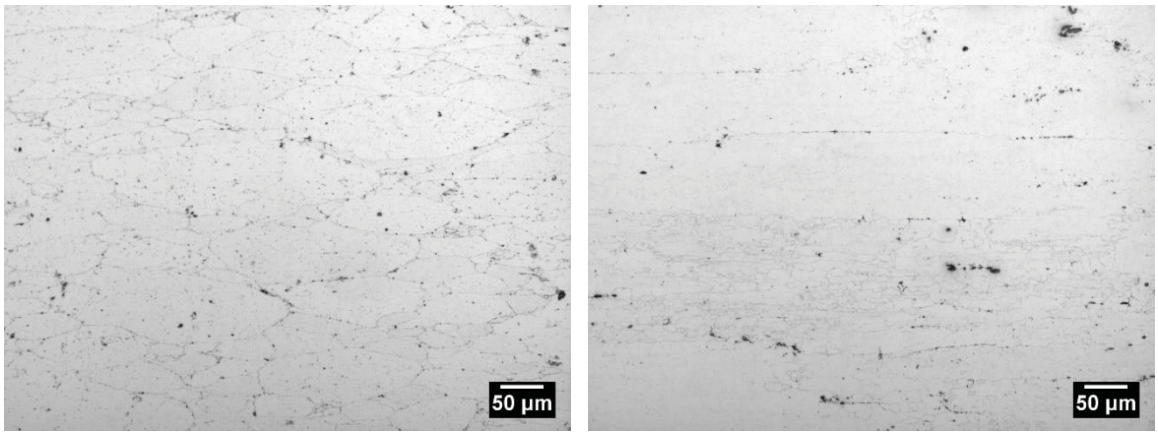

(a) (b)

Figure 40: Microstructure of 7055 specimens (a) SPS-Forged-PA7055-T76 and (b) Wrought 7055-T76.

4.5 Conclusions

The overall objective of this research was to investigate the SPS processing response of gas atomized fully pre-alloyed PA7055 powder. In meeting this objective the following conclusions were reached:

- SPS processing of PA7055 powder at 500°C yielded samples with the highest density and UBS regardless of mode of pressure application.
- When the application of uniaxial pressure was delayed until the sintering temperature was reached (Type II processing) substantial gains in UBS were realized.
- Sintering time was influential on the UBS of Type II processed materials.
- Hot forging of SPS processed billets improved the mechanical properties of PA7055 such that the final values were in reasonable agreement with the wrought counterpart.

4.6 Acknowledgements

The authors would like to graciously acknowledge the financial support provided by Boeing Research and Technology (research contract 11-6392), the Natural Sciences and Engineering Research Council of Canada (NSERC) via collaborative research and development grant #451466 and GKN Sinter Metals. Technical guidance provided by researchers at Boeing (Drs. Steve Gaydos, Ryan Glamm, Marc Froning) is also gratefully acknowledged as is the laboratory assistance provided by colleagues at Dalhousie University (Randy Cooke, Dean Grijm, Dr. Stephen Corbin, Dr. Cathy Whitman) and the powder atomization completed by Dr. Bernd Mais (Ecka Granules).

CHAPTER 5. DISCUSSION AND FUTURE WORK

5.1 Summary

This research was focused on exploring and studying the consolidation of aerospace grade aluminum 7055 powder through conventional (CIP-Sinter) and emerging (SPS) processes. This aluminum powder was used to produce a variety of products which were then characterized to assess density, hardness, tensile properties, bend properties along with metallographic and EBSD inspections. Final products in both cases were processed through a post sintering hot-forging operation and then compared to the wrought 7055 counterpart.

5.1.1 Process Parameter Effects

The following process parameters were investigated based on literature review and aluminum PM experience. The objective was to determine which parameters had the greatest impact and ultimately led to the most promising properties. Of the following parameters some only apply to the CIP-Sinter processing or SPS processing.

5.1.1.1 Pressure

In the case of CIP-Sinter processing, three pressures ranging from 200 to 400MPa were investigated when looking at the effect of pressure on green density. Ultimately a pressure of 400MPa was selected as to ensure that the samples being used in the study had the highest green density and had a good green strength.

With respect to the SPS processing, the sintering pressure itself was kept at 50 MPa and was not investigated but when the pressure was applied it was found to have a great impact on the final product. By producing samples in the Type II processing condition where the pressure was only applied once the sample was heated to the selected temperature, products with much higher UBS were produced.

5.1.1.2 Sintering Temperature

In both cases a number of different sintering temperatures were investigated. In the CIP-Sinter processing, temperatures ranging from 520 to 640°C were investigated while in the SPS processing temperatures up to 500°C were considered. In the CIP-Sinter investigation a liquid was able to be formed during sintering but had to be avoided during SPS sintering. Hence, the range of temperatures differed. In CIP-Sinter processing a sintering temperature of 580°C was found to be optimal while in the SPS processing 500°C was found to produce samples with the highest UBS.

5.1.1.3 Effect of Sintering Aids

The effect of sintering aids was only investigated in the CIP-Sinter processing of PA7055. Two different sintering aids, namely magnesium and tin were investigated and added to the powder mix as blended elemental additions. Magnesium was found to have a detrimental effect on the sintering of the powder and was discarded at the start while an addition of as little as 0.2% tin was found to increase sintered density. Tin was later found to have a negative impact on the tensile properties so it too was discarded as a possible sintering aid.

5.1.1.4 Hold Time

The effect of hold time was only investigated in the SPS processing of PA7055. Here three different hold time ranging from 120 to 2400 seconds were investigated. A hold time of 2400 seconds was found to produce samples with the highest UBS and was related to the increased amount of time available to form strong metal-metal inter-particle bonds.

5.1.1.5 Particle Size

In the CIP-Sinter processing of 7055 two different particle cuts were investigated, namely As-Received and >45µm. While samples produced with the As-Received powder were found to have a slightly higher apparent, green and sinter density they were shown to have a tendency to crack during forging. As such, the >45µm powder cut was selected as optimal for this particular manner of processing.

In the SPS processing of PA7055 a number of narrow particle size cuts were investigated and compared against samples produced with >45μm powder. Although small gains were seen by using powders in the range of 75-150μm, they were not great enough to justify the loss of nearly 80% of the powder during screening. Hence, the >45μm powder was the most practical raw material for both processing technologies.

5.1.2 Secondary Operations

5.1.2.1 Forging

In both studies, sintered products were forged in an attempt to increase the mechanical properties. In CIP-Sinter processing two powder cuts and three different forging temperatures were investigated. Here it was found that products produced with as-received powder had a tendency to crack during forging and thus were not appropriate. Furthermore a forging temperature of 580°C was found to be optimal. In the SPS processing a forging temperature of 580°C was utilized based on the CIP-Sinter findings. In both studies forging was found to greatly increase the tensile properties of the material to levels comparable to wrought 7055-T76.

5.2 Future Work

The subjects listed in this section are recommendations for future work.

- Investigation into the forging behavior of aluminum PM products. This investigation should be split into two sections as follows as to ensure industrial relevance:
    - The first area of study should focus on powder forging parameters with an emphasis on billet parameters such as density and temperature. This is viewed as a strategic direction as a lower sinter density is often specifically targeted when making ferrous sinter-forge parts.

    - The second area of the study should take the findings of the first and then apply and optimize them for use in an industrial setting. At this point more complex, upset forging should be looked at along with low strain forging.
- Perform an investigation on the fatigue behavior of both CIP-Sinter-Forged and SPS-Forged products as the fatigue behavior is very important for aerospace applications.

REFERENCES

[1] "Alloy and Temper Designation Systems for Aluminum - ANSI H35.1." American National Standards Institute.

[2] L. A. Abel, R. T. Kiepura, P. Thomas, H. F. Lampman, and N. D. Wheaton, Eds., *Metals Handbook: Properties and Selection: Nonferrous Alloys and Special-Purpose Materials*, Tenth. 1990.

[3] W. D. J. Callister, *Materials Science and Engineering An Introduction*, Seventh. John Wiley & Son, Inc., 2007.

[4] J. E. Hatch, *Aluminum- Properties and Physical Metallurgy*. American Society for Metals, 1984.

[5] C. Mondal and A. K. Mukhopadhyay, "On the nature of T(Al2Mg3Zn3) and S(Al2CuMg) phases present in as-cast and annealed 7055 aluminum alloy," *Mater. Sci. Eng. A*, vol. 391, no. 1–2, pp. 367–376, Jan. 2005.

[6] L. . Berg, J. Gjønnes, V. Hansen, X. . Li, M. Knutson-Wedel, G. Waterloo, D. Schryvers, and L. . Wallenberg, "GP-zones in Al–Zn–Mg alloys and their role in artificial aging," *Acta Mater.*, vol. 49, no. 17, pp. 3443–3451, Oct. 2001.

[7] M. J. Starink, X. M. Li, I. Introduction, and A. Aims, "A Model for the Electrical Conductivity of Peak-Aged and Overaged Al-Zn-Mg-Cu Alloys," vol. 34, no. April, pp. 899–911, 2003.

[8] V. Hansen, K. Stiller, and G. Waterloo, "Structures and transformations during artificial aging of an industrial 7xxx-Series Al-Zn-Mg-Zr alloy," *Mater. Sci. ...*, pp. 815–820, 2002.

[9] G. Waterloo, V. Hansen, J. Gjønnes, and S. R. Skjervold, "Effect of predeformation and preaging at room temperature in Al–Zn–Mg–(Cu,Zr) alloys," *Mater. Sci. Eng. A*, vol. 303, no. 1–2, pp. 226–233, May 2001.

[10] A. Guinier, "Age-Hardening of a Copper-Aluminum Alloy of Very High Purity," *Inst. Met.*, vol. 838, pp. 177–193, 1939.

[11] G. D. Preston, “The Diffraction of X-Rays by Age-Hardening Aluminium Copper Alloys,” *Proc. R. Soc. A Math. Phys. Eng. Sci.*, vol. 167, no. 931, pp. 526–538, Sep. 1938.

[12] W. F. Smith, *Structure and Properties of Engineering Alloys*, Second. McGraw-Hill, 1993.

[13] J. Chen, L. Zhen, S. Yang, W. Shao, and S. Dai, “Investigation of precipitation behavior and related hardening in AA 7055 aluminum alloy,” *Mater. Sci. Eng. A*, vol. 500, no. 1–2, pp. 34–42, Jan. 2009.

[14] N. Ryum, “Precipitation kinetics in an Al-Zn-Mg alloy,” *Zeitschrift fur Met.*, 1975.

[15] K. Stiller, P. Warren, V. Hansen, J. Angenete, and J. Gjønnes, “Investigation of precipitation in an Al–Zn–Mg alloy after two-step ageing treatment at 100° and 150°C,” *Mater. Sci. Eng. A*, vol. 270, no. 1, pp. 55–63, Sep. 1999.

[16] K. Stiller, V. Hansen, M. Knutson-Wedel, G. Waterloo, and J. Gjønnes, “Hardening Precipitates and their Precursors in 7xxx Alloys,” in *Aluminum Alloys: Their Physical and Mechanical Properties: Proceedings of the 6th Internation Conference on Aluminum Alloys*, 1998, pp. 615–620.

[17] X. Z. Li, V. Hansen, J. GjØnnes, and L. R. Wallenberg, “HREM study and structure modeling of the η′ phase, the hardening precipitates in commercial Al–Zn–Mg alloys,” *Acta Mater.*, vol. 47, no. 9, pp. 2651–2659, Jul. 1999.

[18] G. Sha and A. Cerezo, “Early-stage precipitation in Al–Zn–Mg–Cu alloy (7050),” *Acta Mater.*, vol. 52, no. 15, pp. 4503–4516, Sep. 2004.

[19] X. J. Jiang, B. Noble, B. Holme, G. Waterloo, and J. Tafto, “Differential Scanning Calorimetry and Electron Diffraction Investigation on Low-Temperature Aging in Al-Zn-Mg Alloys,” vol. 31, no. February, pp. 339–348, 2000.

[20] J. G. Kaufman, “Aluminum Alloy Database.” Knovel, 2009.

[21] B. Sarkar, M. Marek, and E. A. Starke, “The effect of copper content and heat treatment on the stress corrosion characteristics of Ai-6Zn-2Mg-X Cu alloys,” *Metall. Trans. A*, vol. 12, no. 11, pp. 1939–1943, Nov. 1981.

[22] A. Deschamps, Y. Bréchet, and F. Livet, “Influence of copper addition on precipitation kinetics and hardening in Al–Zn–Mg alloy,” *Mater. Sci. Technol.*, vol. 15, no. 9, pp. 993–1000, Sep. 1999.

[23] G. Sha and A. Cerezo, “Characterization of precipitates in an aged 7xxx series Al alloy,” *Surf. Interface Anal.*, vol. 36, no. 56, pp. 564–568, May 2004.

[24] J. Liu, “Advanced Aluminium and Hybrid Aerostructures for Future Aircraft,” *Mater. Sci. Forum*, vol. 519–521, pp. 1233–1238, 2006.

[25] A. Heinz, A. Haszler, C. Keidel, S. Moldenhauer, R. Benedictus, and W. . Miller, “Recent development in aluminium alloys for aerospace applications,” *Mater. Sci. Eng. A*, vol. 280, no. 1, pp. 102–107, Mar. 2000.

[26] X. Li, B. Xiong, Y. Zhang, C. Hua, F. Wang, B. Zhu, and H. Liu, “Effect of one-step aging on microstructure and properties of a novel Al-Zn-Mg-Cu-Zr alloy,” *Sci. China Ser. E Technol. Sci.*, vol. 52, no. 1, pp. 67–71, Jan. 2009.

[27] “Alcoa.” [Online]. Available: https://www.alcoa.com/global/en/home.asp.

[28] R. M. German, *Powder Metallurgy Science*. Metal Powder Industries Federation, 1994.

[29] R. M. German, P. Suri, and S. J. Park, “Review: liquid phase sintering,” *J. Mater. Sci.*, vol. 44, no. 1, pp. 1–39, Dec. 2008.

[30] G. Schaffer, B. Hall, S. Bonner, S. Huo, and T. Sercombe, “The effect of the atmosphere and the role of pore filling on the sintering of aluminium,” *Acta Mater.*, vol. 54, pp. 131–138, Oct. 2005.

[31] I. A. MacAskill, R. L. Hexemer, I. W. Donaldson, and D. P. Bishop, “Effects of magnesium, tin and nitrogen on the sintering response of aluminum powder,” *J. Mater. Process. Technol.*, vol. 210, no. 15, pp. 2252–2260, Nov. 2010.

[32] T. B. Sercombe and G. B. Schaffer, “On the role of tin in the nitridation of aluminium powder,” *Scr. Mater.*, vol. 55, no. 4, pp. 323–326, Aug. 2006.

[33] G. B. Schaffer, J.-Y. Yao, S. J. Bonner, E. Crossin, S. J. Pas, and a.J. Hill, “The effect of tin and nitrogen on liquid phase sintering of Al–Cu–Mg–Si alloys,” *Acta Mater.*, vol. 56, no. 11, pp. 2615–2624, Jun. 2008.

[34] G. B. Schaffer, T. B. Sercombe, and R. N. Lumley, “Liquid phase sintering of aluminium alloys,” *Mater. Chem. Phys.*, vol. 67, no. 1–3, pp. 85–91, Jan. 2001.

[35] R. M. German, “Supersolidus Liquid-Phase Sintering of Prealloyed Powders,” vol. 28, no. July, pp. 1553–1567, 1997.

[36] Y. Liu, R. Tandon, and R. M. German, “Modeling of Supersolidus Liquid Phase Sintering: II. Densification,” vol. 26, no. September, 1995.

[37] R. M. German, “An Update on the Theory of Supersolidus Liquid Phase Sintering.pdf.” .

[38] S. Kalpakjian, *Manufacturing Processes for Engineering Materials*, Second Edi. Addison-Wesley Publishing Company, 1992.

[39] T. Altan, G. Ngaile, and G. Shen, Eds., *Cold and Hot Forging: Fundamentals and Applications*. ASM International, 2005.

[40] A. Bose and W. B. Einsen, *Hot Consolidation of Powders and Particulates*. Metal Powder Industries Federation, 2003.

[41] I. A. MacAskill, a. D. P. LaDepha, J. H. Milligan, J. J. Fulton, and D. P. Bishop, “Effects of cold and hot densification on the mechanical properties of a 7XXX series powder metallurgy alloy,” *Powder Metall.*, vol. 52, no. 4, pp. 304–310, Dec. 2009.

[42] R. E. D. Mann, R. L. Hexemer, I. W. Donaldson, and D. P. Bishop, “Hot deformation of an Al–Cu–Mg powder metallurgy alloy,” *Mater. Sci. Eng. A*, vol. 528, no. 16–17, pp. 5476–5483, Jun. 2011.

[43] W. G. E. Mosher, G. J. Kipouros, W. F. Caley, I. W. Donaldson, and D. P. Bishop, “On hot deformation of aluminium-silicon powder metallurgy alloys,” *Powder Metall.*, vol. 54, no. 3, pp. 366–375, Jul. 2011.

[44] D. P. Bishop, W. F. Caley, G. J. Kipouros, R. L. Hexemer, and I. W. Donaldson, “Powder metallurgy processing of 2xxx and 7xxx series aluminium alloys,” *Can. Metall. Q.*, vol. 50, no. 3, pp. 246–252, Jul. 2011.

[45] R. Cooke and G. Steedman, “Preliminary studies on the development of hot-forged aluminium PM technology,” *Adv. ...*, 2013.

[46] Ducker Worldwide, “2015 North American Light Vehicle Aluminum Content Study - Executive Summary,” 2014.

[47] P. Ramakrishan, “Automotive applications of powder metallurgy,” in *Advances in Powder Metallurgy: Properties, Processing and Applications*, Woodhead Publishing Limited, 2013, pp. 493–519.

[48] S. Huo, B. Heath, and D. Ryan, “Applications of Powder Metallurgy Aluminums for Automotive Valve-Trains,” *SAE Int. J. Mater. Manuf.*, vol. 1, no. 1, pp. 511–515, Apr. 2008.

[49] G. N. Grayson, G. B. Schaffer, and J. R. Griffiths, “On the Fatigue of Sintered Aluminium Alloys,” vol. 28, pp. 981–985, 2004.

[50] Y.-W. Kim, W. M. Griffith, and F. H. Froes, “Surface Oxides in P/M Aluminum Alloys,” *JOM*, vol. 37, no. 8, pp. 27–33, Oct. 1985.

[51] A. S. Chua, M. Brochu, and D. P. Bishop, “Spark plasma sintering of prealloyed aluminium powders,” *Powder Metall.*, vol. 58, no. 1, pp. 51–60, Mar. 2015.

[52] J. E. Garay, "Current-Activated, Pressure-Assisted Densification of Materials," *Annu. Rev. Mater. Res.*, vol. 40, no. 1, pp. 445–468, Jun. 2010.

[53] Z. A. Munir, U. Anselmi-Tamburini, and M. Ohyanagi, "The effect of electric field and pressure on the synthesis and consolidation of materials: A review of the spark plasma sintering method," *J. Mater. Sci.*, vol. 41, no. 3, pp. 763–777, Feb. 2006.

[54] R. Orrù, R. Licheri, A. M. Locci, A. Cincotti, and G. Cao, "Consolidation/synthesis of materials by electric current activated/assisted sintering," *Mater. Sci. Eng. R Reports*, vol. 63, no. 4–6, pp. 127–287, Feb. 2009.

[55] S.-X. Song, Z. Wang, and G.-P. Shi, "Heating mechanism of spark plasma sintering," *Ceram. Int.*, vol. 39, no. 2, pp. 1393–1396, Mar. 2013.

[56] S. Diouf and A. Molinari, "Densification mechanisms in spark plasma sintering: Effect of particle size and pressure," *Powder Technol.*, vol. 221, pp. 220–227, May 2012.

[57] E. A. Olevsky, S. Kandukuri, and L. Froyen, "Consolidation enhancement in spark-plasma sintering: Impact of high heating rates," *J. Appl. Phys.*, vol. 102, no. 11, p. 114913, 2007.

[58] U. Anselmi-Tamburini, J. E. Garay, and Z. A. Munir, "Fast low-temperature consolidation of bulk nanometric ceramic materials," *Scr. Mater.*, vol. 54, no. 5, pp. 823–828, Mar. 2006.

[59] N. Bertolino, J. Garay, U. Anselmi-Tamburini, and Z. A. Munir, "Electromigration effects in Al-Au multilayers," *Scr. Mater.*, vol. 44, no. 5, pp. 737–742, Mar. 2001.

[60] N. Bertolino, J. Garay, U. Anselmi-Tamburini, and Z. A. Munir, "High-flux current effects in interfacial reactions in Au-Al multilayers," *Philos. Mag. B*, vol. 82, no. 8, pp. 969–985, May 2002.

[61] J. E. Garay, U. Anselmi-Tamburini, and Z. A. Munir, "Enhanced growth of intermetallic phases in the Ni–Ti system by current effects," *Acta Mater.*, vol. 51, no. 15, pp. 4487–4495, Sep. 2003.

[62] P. Asoka-Kumar, K. O'Brien, K. G. Lynn, P. J. Simpson, and K. P. Rodbell, "Detection of current-induced vacancies in thin aluminum–copper lines using positrons," *Appl. Phys. Lett.*, vol. 68, no. 3, p. 406, 1996.

[63] W. Chen, U. Anselmi-Tamburini, J. E. Garay, J. R. Groza, and Z. A. Munir, "Fundamental investigations on the spark plasma sintering/synthesis process I," *Mater. Sci. Eng. A*, vol. 394, no. 1–2, pp. 132–138, Mar. 2005.

[64] U. Anselmi-Tamburini, J. E. Garay, and Z. A. Munir, "Fundamental investigations on the spark plasma sintering/synthesis process III," *Mater. Sci. Eng. A*, vol. 407, no. 1–2, pp. 24–30, Oct. 2005.

[65] M. Z. Kol'chinskli, N. F. Medvedenko, and F. P. Gnatush, "Electric-Discharge Sintering of Mixtures of Aluminum and Copper Powders," vol. 7, no. 7, pp. 13–16, 1977.

[66] G. Xie, O. Ohashi, T. Yoshioka, M. Song, and K. Mitsuishi, "Effect of Interface Behavior between Particles on Properties of Pure Al Powder Compacts by Spark Plasma Sintering," *Mater. Trans.*, vol. 42, no. 9, pp. 1846–1849, 2001.

[67] G. Xie, O. Ohashi, N. Yamaguchi, M. Song, K. Mitsuishi, K. Furuya, and T. Noda, "Reduction of Surface Oxide Films in Al–Mg Alloy Powders by Pulse Electric Current Sintering," *J. Mater. Res.*, vol. 19, no. 03, pp. 815–819, Mar. 2011.

[68] G. Xie, O. Ohashi, M. Song, K. Furuya, and T. Noda, "Behavior of Oxide Film at the Interface between Particles in Sintered Al Powders by Pulse Electric-Current Sintering," vol. 34, no. March, pp. 699–703, 2003.

[69] G. Xie, O. Ohashi, N. Yamaguchi, M. Song, K. Furuya, and T. Noda, "Characterization of Interface between Particles in Al Powder Compacts by Pulse Electric Current Sintering," *Mater. Sci. Forum*, vol. 423–425, pp. 97–102, 2003.

[70] G. Xie, O. Ohashi, K. Chiba, N. Yamaguchi, M. Song, K. Furuya, and T. Noda, "Frequency effect on pulse electric current sintering process of pure aluminum powder," *Mater. Sci. Eng. A*, vol. 359, no. 1–2, pp. 384–390, Oct. 2003.

[71] M. Zadra, F. Casari, L. Girardini, and A. Molinari, “Spark plasma sintering of pure aluminium powder: mechanical properties and fracture analysis,” *Powder Metall.*, vol. 50, no. 1, pp. 40–45, Mar. 2007.

[72] H. Kwon, D. H. Park, Y. Park, J. F. Silvain, A. Kawasaki, and Y. Park, “Spark plasma sintering behavior of pure aluminum depending on various sintering temperatures,” *Met. Mater. Int.*, vol. 16, no. 1, pp. 71–75, Feb. 2010.

[73] G. A. Sweet, M. Brochu, R. L. Hexemer, I. W. Donaldson, and D. P. Bishop, “Microstructure and mechanical properties of air atomized aluminum powder consolidated via spark plasma sintering,” *Mater. Sci. Eng. A*, vol. 608, pp. 273–282, Jul. 2014.

[74] R. Zheng, Y. Sun, K. Ameyama, and C. Ma, “Optimizing the strength and ductility of spark plasma sintered Al 2024 alloy by conventional thermo-mechanical treatment,” *Mater. Sci. Eng. A*, vol. 590, pp. 147–152, Jan. 2014.

[75] R. Vintila, A. Charest, R. A. L. Drew, and M. Brochu, “Synthesis and consolidation via spark plasma sintering of nanostructured Al-5356/B4C composite,” *Mater. Sci. Eng. A*, vol. 528, no. 13–14, pp. 4395–4407, May 2011.

[76] J. Ye, L. Ajdelsztajn, and J. M. Schoenung, “Bulk nanocrystalline aluminum 5083 alloy fabricated by a novel technique: Cryomilling and spark plasma sintering,” *Metall. Mater. Trans. A*, vol. 37, no. 8, pp. 2569–2579, Aug. 2006.

[77] S. Rudinsky, J. M. Aguirre, G. Sweet, J. Milligan, D. P. Bishop, and M. Brochu, “Spark plasma sintering of an Al-based powder blend,” *Mater. Sci. Eng. A*, vol. 621, pp. 18–27, Jan. 2015.

[78] H. Chen and B. Yang, “Effect of Preipiations on Microstructures and Mechanical Properties of Nanostructured Al-Zn-Mg-Cu Alloy,” *Mater. Trans.*, vol. 49, no. 12, pp. 2912–2915, 2008.

[79] C. D. Turner and M. F. Ashby, “The cold isostatic pressing of composite powders—I. Experimental investigations using model powders,” *Acta Mater.*, vol. 44, no. 11, pp. 4521–4530, Nov. 1996.

[80] A. S. Chua, D. P. Bishop, R. J. Glamm, R. L. Hexemer, and I. W. Donaldson, "A comparison of industrial processing strategies utilized to consolidate aluminum powder metallurgy alloys with aerospace relevant chemistries," in *Advances in Powder Metallurgy and Particulate Materials*, 2014, pp. 7127–7137.

[81] R. W. Cooke, G. Steedman, D. P. Bishop, R. L. Hexemer, and I. W. Donaldson, "Preliminary studies on the development of hot-forged aluminum PM technology," in *Advances in Powder Metallurgy and Particulate Materials*, 2013, pp. 3108–3119.

[82] D. P. Bishop, B. Hofmann, and K. R. Couchman, "Properties and Attributes of Commercially Available AC2014-Type Aluminum P/M Alloys," in *Advances in Powder Metallurgy and Particulate Materials*, 2000, pp. 87–100.

[83] C. D. Boland, D. P. Bishop, R. L. Hexemer, and I. W. Donaldson, "On the development of an aluminum PM alloy for 'press-sinter- size' technology," in *Advances in Powder Metallurgy and Particulate Materials*, 2010, pp. 764–777.

[84] A. S. Chua and D. P. Bishop, "Effects of Compaction Technique on the Processing Response of Aluminum PM Alloys," *Can. Metall. Q.*, vol. 53, no. 4, pp. 407–415, 2014.

[85] K. Matsugi, Y. Wang, T. Hatayama, O. Yanagisawa, and M. Kiritani, "Rapid Consolidation by Spark Sintering of Rapidly Solidified 7075 Aluminum Alloy Powder," *Radiat. Eff. Defects Solids*, vol. 157, no. 1–2, pp. 233–244, Oct. 2002.

[86] D. Liu, Y. Xiong, T. D. Topping, Y. Zhou, C. Haines, J. Paras, D. Martin, D. Kapoor, J. M. Schoenung, and E. J. Lavernia, "Spark Plasma Sintering of Cryomilled Nanocrystalline Al Alloy - Part II: Influence of Processing Conditions on Densification and Properties," *Metall. Mater. Trans. A*, vol. 43, no. 1, pp. 340–350, Aug. 2011.

[87] G. A. Sweet, M. Brochu, R. L. Hexemer, I. W. Donaldson, and D. P. Bishop, "Consolidation of aluminum-based metal matrix composites via spark plasma sintering," *Mater. Sci. Eng. A*, vol. 648, pp. 123–133, Nov. 2015.

[88] B. E. Hayden, W. Wyrobisch, W. Oppermann, S. Hachicha, P. Hofmann, and A. M. Bradshaw, “The interaction of oxygen with aluminium: Mainly ellipsometric aspects,” *Surf. Sci.*, vol. 109, no. 1, pp. 207–220, Aug. 1981.

[89] A. I. Litvintsev and L. A. Arbuzova, “Kinetics of degassing of aluminum powders,” *Sov. Powder Metall. Met. Ceram.*, vol. 6, no. 1, pp. 1–10, Jan. 1967.

[90] Z. Zhang, S. Dallek, R. Vogt, Y. Li, T. D. Topping, Y. Zhou, J. M. Schoenung, and E. J. Lavernia, “Degassing Behavior of Nanostructured Al and Its Composites,” *Metall. Mater. Trans. A*, vol. 41, no. 2, pp. 532–541, Nov. 2009.

[91] M. Yamasaki and Y. Kawamura, “Effect of Vacuum Degassing on Surface Characteristics of Rapidly Solidified Al-Based Alloy Powders,” *Mater. Trans.*, vol. 45, no. 4, pp. 1335–1338, 2004.

[92] M. Yamasaki and Y. Kawamura, “Changes in the Surface Characteristics of Gas-Atomized Pure Aluminum Powder during Vacuum Degassing,” *Mater. Trans.*, vol. 47, no. 8, pp. 1902–1905, 2006.

[93] J. H. Dudas and C. B. Thompson, “Improved Sintering Procedures for Aluminum P/M,” in *International Powder Metallurgy Conference*, 1970, pp. 19–36.

[94] J. . Martín and F. Castro, “Liquid phase sintering of P/M aluminium alloys: effect of processing conditions,” *J. Mater. Process. Technol.*, vol. 143–144, pp. 814–821, Dec. 2003.

[95] N. P. Kraus, D. P. Bishop, R. L. Hexemer, and I. W. Donaldson, “Consolidation of Aerospace Grade Aluminum 7055 Powder Via Sinter-Forge Processing,” in *Advances in Powder Metallurgy and Particulate Materials*, 2016.

APPENDIX A: COPYRIGHT RELEASE

5.3 MPIF Release

May 30 2016

PowderMet 2016, the International Conference on Powder Metallurgy and Particulate Materials Proceedings
Metal Powder Industries Federation
105 College Road East
Prinston, NJ 08540-6692

I am preparing my MASc thesis for submission to the Faculty of Graduate Studies at Dalhousie University, Halifax, Nova Scotia, Canada. I am seeking your permission to include a manuscript version of the following paper(s) as a chapter in the thesis:

CONSOLIDATION OF AEROSPACE GRADE ALUMINUM 7055 POWDER VIA SINTER-FORGE PROCESSING, N.P. Kraus, D.P. Bishop, R.L. Hexemer Jr. and I.W. Donaldson

Canadian graduate theses are reproduced by the Library and Archives of Canada (formerly National Library of Canada) through a non-exclusive, world-wide license to reproduce, loan, distribute, or sell theses. I am also seeking your permission for the material described above to be reproduced and distributed by the LAC(NLC). Further details about the LAC(NLC) thesis program are available on the LAC(NLC) website (www.nlc-bnc.ca).

Full publication details and a copy of this permission letter will be included in the thesis.

Yours sincerely,

Neal Kraus

Permission is granted for:

a) the inclusion of the material described above in your thesis.

b) for the material described above to be included in the copy of your thesis that is sent to the Library and Archives of Canada (formerly National Library of Canada) for reproduction and distribution.

Name: James P. Adams Title: VP, Technical Services

Signature: [redacted] Date: 5/31/16